ORIGINAL ARTICLE
DOI: https://doi.org/10.18599/grs.2025.4.7

Interpretation of Lineaments Within the Western Part of the Baikal-Patom Belt Using a Multiscale Tectonophysical Approach in the Context of Ore-Forming Systems Prediction

S.A. Ustinov[*], *V.A. Petrov, A.A. Andreev, A.D. Svecherevsky, I.A. Kochkin, V.V. Shukhov*
Institute of Geology of Ore Deposits, Petrography, Mineralogy and Geochemistry of the Russian Academy of Sciences, Moscow, Russian Federation

Abstract. In the article, using the territory of the western part of the Baikal-Patom belt as an example, an author's approach to the automatic extraction of lineaments reflecting various scale levels of the development of the fault network framework is proposed, based on the sequential lowering of the spatial resolution of the FABDEM digital elevation model. The results of a comprehensive spatial-geometric analysis of the extracted lineaments, marking fault structures of various ranks, are presented. Based on correlation analysis, groups of structures unambiguously corresponding to a definite scale level are identified. For the reconstruction of the parameters of the stress-strain state, the kinematics of the proposed fault structures, and the restoration of the sequence of tectogenesis stages, the paragenesis of structures identified at each stage of generalization of the digital elevation model was interpreted based on the shear model proposed by P.L. Hancock. As a result, in the history of the geological development of the territory, three sequential stages of tectogenesis have been established, characterized by: I) sub-latitudinal – east-northeastern, II) northeastern, and III) northwestern orientations of the axis of maximum compression. The first stage is manifested at all scale levels and corresponds to the processes of accretionary-collisional interaction of the margin of the Siberian craton with microcontinents and island-arc terranes. The second and third stages are manifested exclusively at the local level and correlate with the formation of sub-latitudinal strike-slips and thrusts in the northwestern direction. The obtained results, based on the calculation of the tendency-to-shear coefficient and visualization of the most hydraulically active segments of the fault structures, formed the basis for creating multiscale predictive-prospecting models of mineral resources of the territory, taking into account the identified stages of tectogenesis. It has been established that the first and second stages played the greatest role in the localization of metallic ore mineralization. In this case, the accuracy of the complex model amounted to 94%.

Keywords: Earth remote sensing, digital elevation model, lineament analysis, fault, tectonophysical analysis, structural-geomorphological method, stress-strain state, predictive and prospecting model of ore minerals, Baikal folded region, Baikal-Patom belt

Recommended citation: Ustinov S.A., Petrov V.A., Andreev A.A., Svecherevsky A.D., Kochkin I.A., Shukhov V.V. (2025). Interpretation of Lineaments Within the Western Part of the Baikal-Patom Belt Using a Multiscale Tectonophysical Approach in the Context of Ore-Forming Systems Prediction. *Georesursy = Georesources*, 27(4), pp. 83–106. https://doi.org/10.18599/grs.2025.4.7

Introduction

Discontinuous structures (faults, fractures) in the Earth's crust, which in the most general definition represent a loss of continuity in rock massif with or without displacement along the plane of rupture, have formed throughout the entire geological history of the Earth depending on the geodynamic settings active at specific time. These structures form tectonically weakened zones, act as boundaries of lithospheric plates and tectonic blocks of the Earth's crust, along which their movement occurs or has occurred, and are also of great importance as pathways and channels for the influx of deep mantle material or fluids into near-surface areas and to the Earth's surface. Furthermore, faults can be ancient,

[*]Corresponding author: Stepan A. Ustinov
e-mail: stevesa@mail.ru

active at a certain stage of geological history, or can exhibit seismic activity at present, periodically leading to the occurrence of earthquake focus (Sherman, 2014).

It is important to note that faults in the Earth's crust form not only under the influence of regional tectonic stresses, but also as a result of global processes associated with planetary fracturing and rheological features of rocks. Planetary fracturing, caused by global-scale stresses, creates a system of tectonically weakened zones that can be inherited at various scale levels – from microcracks to regional faults (Kats et al., 1986; Anders, Wiltschko, 1994; Sherman, 2014). These structures often act as the basis for subsequent tectonic activation, determining the orientation and morphology of newly formed fractures.

The rheological properties of rocks, such as viscosity, strength, and anisotropy, play a key role in the localization of deformations. For example, brittle rocks (granites, quartzites) tend to form discrete faults with clear slip planes, while sequences with ductile properties (clay shales, rock salt) deform through folding or flow, forming zones of cleavage or schistosity (Faulkner et al., 2011). In addition, changes in rheological parameters with depth (transition from brittle to ductile behavior) control the vertical segmentation of fault zones, which is important for understanding their fluid-conducting function (Faulkner et al., 2018).

Despite the vast number of works investigating the mechanisms of fault formation, their description, classification, and tectonophysical interpretation, and the development of numerous methods for structural-geological and tectonic mapping, the task of mass identification and classification of faults over extensive areas remains quite difficult for implementation. The most reliable method is still field geological studies with verification of identified structures through mining excavations (ditches, boreholes). However, such investigations, due to significant costs and considering expediency (for example, for the purpose of mineral exploration), are typically conducted only within small areas – prospective and promising sites for various types of mineral resources (MR): deposits, ore fields, and their flanks.

For mapping fault structures within more extensive territories, various geophysical (ground-based, aerial and unmanned aerial surveys) methods are used, the results of interpretation of which in the context of identifying tectonic structures, especially of different ages and ranks, are also not always unambiguous. The results of applying the listed methods are often used in compiling multi-scale state geological maps (SGM). For these maps, a collection, analysis, and generalization of all available geological information for the territory are carried out, covering not only rock types and ages but also fault tectonics. This leads to the fact that the fault framework represented on the SGMs being segmented and, to varying degrees, understudied.

For identifying fault structures within extensive areas, lineament analysis is often applied. The term "lineament" was proposed by the American geologist W. Hobbs over a hundred years ago (Hobbs, 1904). This definition is directly related to the morphological features of the Earth's surface. In the classical sense, it refers to straight-line negative relief forms, exposed straight slopes, scarps and ledges, sequences of rectilinear segments of small watercourses crossing in one direction watersheds and valleys, rectilinear axial lines of watersheds, and areas of contour lines concentration and inflection. Considering controversial issues concerning the evolution of the Earth's terrain, some geologists are highly skeptical about lineament analysis. Some researchers believe that relief features reflect only young (neotectonic) fault structures and cannot be used to reconstruct ancient tectonic stages (Burtman et al., 1980; Makarov, 2008). Others agree that the relief evolved throughout the entire geological history and can reflect ancient, most manifested periods of tectogenesis (Kats et al., 1986; Vidyapin, Bondar, 2021; Ustinov et al., 2024a). There is also the question of the reliability of identifying a fault based on marked lineaments. Undoubtedly, the relief has been subjected to exogenous processes, including erosion, throughout its evolution. However, the authors of this article, based on their extensive experience in identification of geological structures, believe that not every lineament (especially a short one) reflects a fault zone, but every axial line (displacement plane) of an extensive fault reaching the surface will be marked by a lineament. Due to the absence of other methods for reliable mass identification of fault structures, lineament analysis can be considered as the most effective remote approach for reconstructing the fault framework and deep tectonic architecture within extensive territories (Kats et al., 1986).

At the current stage of scientific and technological development, with the launch of numerous spacecraft, opportunities for acquiring and analyzing diverse Earth remote sensing data, including radio-locational, multi- and hyper-spectral imaging have emerged. Structural-lineament analysis can be carried out based on the three-dimensional visualization of the Earth's surface elevation. For this, results from space radar topographic surveys, which enable the creation of Digital Elevation Models (DEM), can be used. Lineaments on a DEM are identified using either manual or automated methods.

It should be noted that in most studies lineaments are identified using single- or multi-channel satellite imagery, where terrain features are not always clearly traced, and even vegetation boundaries are sometimes

identified as linear objects, leading to significant errors. Furthermore, there is no generally accepted methodology for interpreting the results of identifying a network of lineaments in geodynamic, tectonic, and tectonophysical contexts.

In addition, in the practice of structural-lineament analysis, researchers most often identify single-rank lineaments, typically short ones, without taking into account the scale effect in the development of interpreted fault structures. This effect consists of "the change in any properties of natural or artificial objects and materials when their geometric parameters are varied", which is also true for faults (Faulkner et al., 2011; Petrov et al., 2017; Petrov et al., 2019). As numerous model experiments have shown, during the formation of an extensive fault zone, systems and echelons of associated cracks of various kinematic types and different ranks, reflecting a specific scale level, develop in a certain sequence.

In the presented study, using the western part of the Baikal-Patom belt as an example, a methodology for interpreting the spatial position of lineaments has been developed and validated. This methodology, based on structural-geomorphological, spatial-geometric, spatial-density, and tectonophysical approaches, allows not only to identify parameters of shear-related tectonodynamic processes manifesting at different scales but also to establish specific features of the development of the multi-rank fault structures framework that control the localization of ore objects within the territory. This opens up possibilities for creating multi-scale structural prospecting models (PM) for various types of mineral resources.

Object of study

The Baikal-Patom Belt (BPB), the western part of which is considered as the research object, is a component of the Baikal Folded Area (BFA), which, in turn, is an element of the Central Asian Mobile Belt. Besides the BPB, within the BFA, first-order structures such as the Baikal-Muya Folded Belt (BMB) and the Barguzin-Vitim superterrane are distinguished. Most researchers agree that these structures were formed in a unified sequence of the main tectono-magmatic stages of BFA evolution over the last billion years. A generalized geological and metallogenic scheme of the western part of the BPB is presented in Figure 1.

The structure of the BPB is mainly determined by Neoproterozoic structures composed of a unified carbonate-terrigenous Patom Complex, which was emplaced on the Early Precambrian basement of the Angara and Aldan plates of the Siberian Craton. The basement is exposed within the Chuya, Tonod, and Nechersk granitoid uplifts. In cross-section, the BPB is clearly divided into an external structural zone, corresponding to the marginal trough (the Pribaikalskaya Zone), and the inner zone, which includes continental rifts (the Olokit Zone), internal uplifts (the Mamskaya Zone), and troughs (the Patom, Delyun-Uran, and Bodaibo Zones) (Rytsk et al., 2011). Within the internal structural zone of the BPB, on the Angara Plate, northeastern strikes of sedimentary sequences and linear structures predominate (Fig. 1D), whereas on the Aldan Plate, sublatitudinal and northwestern trends dominate. The formation of the overall BPB structure is attributed either to the primary morphology of the paleobasins of sedimentation (Salop, 1964) or to large-scale deformations that completed at the end of the Early Paleozoic (Zonenshain et al., 1990).

The classical understanding of the tectonic nature of the BPB by most authors is somehow connected with the evolution of the paleoshelf of the passive margin of the Siberian craton and is based on the model of its accretionary-collisional interaction with various microcontinents and island-arc terranes at the end of the Late Precambrian and Early Paleozoic (Gusev, Khain, 1995; Gordienko, 2006; Gordienko et al., 2013; Stanevich et al., 2007; Chugaev et al., 2018; Nikishin et al., 2010). In the study (Zorin et al., 2009), the evolution of the BPB is closely tied to the development of subduction processes in the BMB, and sedimentary complexes are compared with formations of back-arc basins. According to (Khomentovsky, Postnikov, 2001), the evolution of the BPB includes a long period of epicontinental rifting, the passive continental margin of the Baikal-Vitim oceanic basin, the back-arc basin of the Middle Vitim island arc, the residual basin in the rear of the accretion zone and, finally, the foreland basin in the rear of the thrust-fold belt and the completing epicontinental shelf basin at the end of the Late Vendian.

An alternative model also exists. It is based on riftogenic formation of BFA structures and founded on modern geological, geochronological, and isotope-geochemical data obtained over the last decade. According to this model, at the boundary of 790–755 million years (Andreev et al., 2022), a collisional joining of the Anamakit-Muisky terrane, a constituent part of the Barguzin-Vitim superterrane, with the continental margin of the Siberian craton occurred. The collision zone is marked by gneiss-granites of the Early Baikalian complex, which are established in the Goremyka, Muisky, Umolikit, and Vodorazdelny tectonic blocks of the BMB. The consequence of this event was the formation of an accretionary-collisional orogen with recycled ancient continental crust. The Late Riphean is characterized by extension followed by the breakup of the Rodinia supercontinent under the influence of a mantle plume (Kuzmin, Yarmolyuk, 2016).

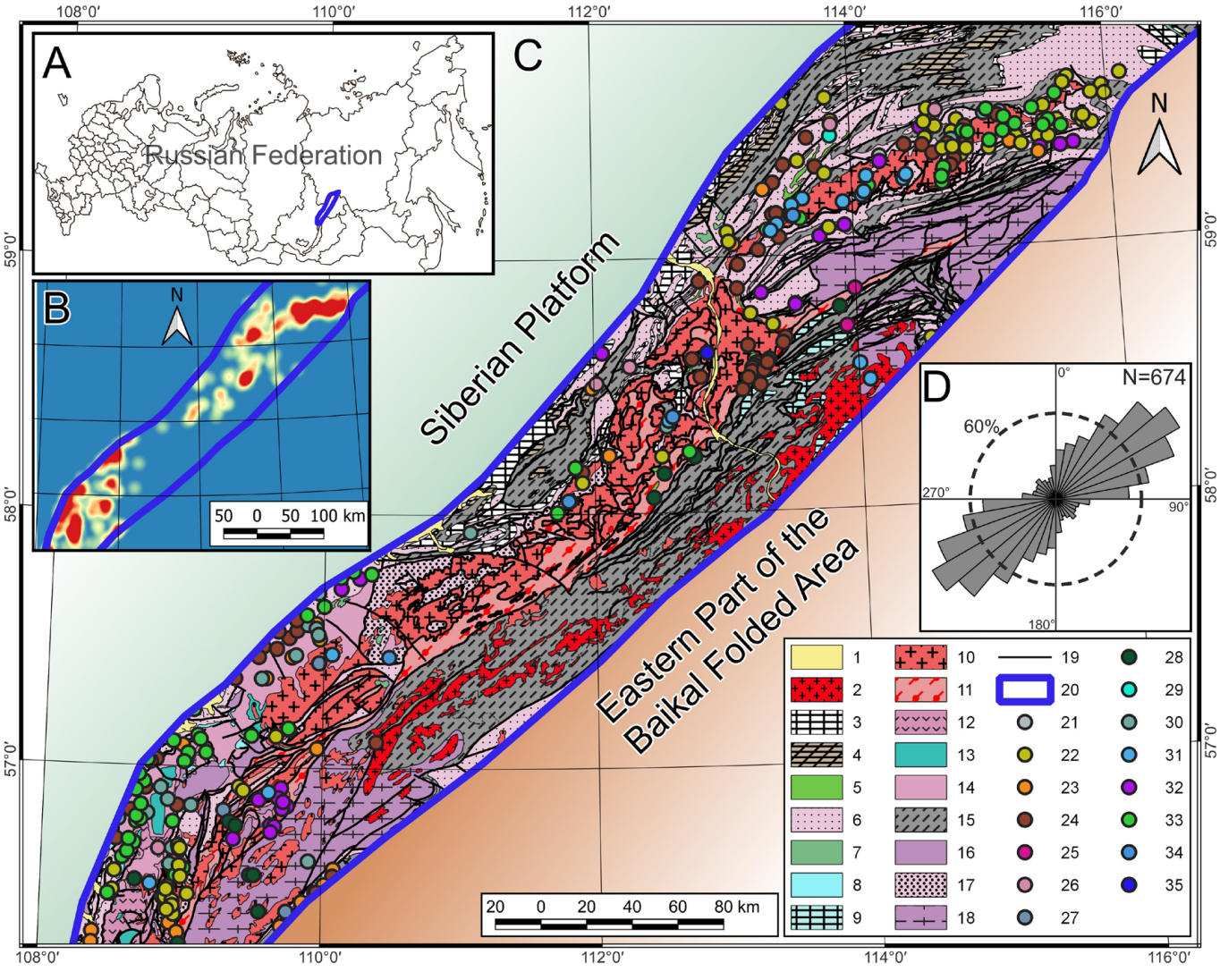

Fig. 1. Materials for the western part of the Baikal-Patom belt generalized by the authors. A – location of the study area relative to the subjects of the Russian Federation. B – relative density of metallic ore mineralization from blue (lowest density of objects) to red (highest density of objects). C – geological-metallogenic map of the western part of the Baikal-Patom belt based on materials from state geological maps (O-49 and O-59) (Makaryev et al., 2010; Mitrofanova et al., 2012): 1 – Neogene-Quaternary deposits; 2 – Mamsky complex of pegmatoid granites and pegmatites (O-S); 3 – carbonate rocks of the Chenchinskaya suite (RF_3); 4 – marls of the Nikolskaya suite (RF_3); 5 – dikes and sills of the Medvezhevsky volcanic complex (RF_2); 6 – volcanic complexes of the Middle Riphean (sandstones, conglomerates, tuffaceous sandstones); 7 – Chaysky complex of moderately alkaline gabbro-dolerites (KR_2); 8 – Parusny monzonite complex (KR_2); 9 – marbles and crystalline limestones of the Konkuderskaya strata (KR_2); 10 – granites of the Chuya-Nechera complex (KR_2); 11 – Malomin dynamometamorphic complex – cataclasites, mylonites, blastomylonites (KR_2); 12 – andesitic volcanic complex (KR_2); 13 – Levodomugda granosyenite complex (KR_2); 14 – trachydacites of the Domugda volcanic complex (KR_2); 15 – shales (KR_2); 16 – rhyodacites of the Khibelen volcanic complex (KR_2); 17 – tuffs of the Bolsheminya volcanic complex (KR_1); 18 – gneisses, granite-gneisses, and shales of the Chuya strata (KR_1:AR_2); 19 – mapped faults; 20 – study area boundary; 21–37 – deposits and ore occurrences of metallic minerals (out of scale): 21 – Ag; 22 – Au; 23 – Cu; 24 – Fe; 25 – Li; 26 – Mn; 27 – Mo; 28 – Nb, Ta; 29 – Ni, Co; 30 – Pb, Zn; 31 – Sn; 32 – Ti; 33 – U; 34 – W; 35 – Zr, Y, Yb. D – rose diagram of orientations of mapped faults: N – number of objects.

The processes of continental rifting of the Early Baikalian stage, which started in the Olokit Zone of the BPB, were completed by the boundary of 660–640 million years with localization of extension in the Kichera Zone of the BMB, which led to the destruction of the Early Precambrian crust and the formation of Late Baikalian juvenile crust in riftogenic structures of varying degrees of opening (Andreev et al., 2022).

At the end of the Late Neoproterozoic, the structural separation of the BFA was completed. As a result, its morphostructure became similar to a "deformed rhombus" – a universal morphotype of tectonic structures formed as a result of shear deformations of the crust (Rytsk, 2020). In the platform area of the Siberian craton, bordering the BFA, the processes of Late Baikalian rifting led to the formation of the Patom-Vilyui paleorift trough and segmented troughs of the Angaro-Lena (Pribaikalskaya) Zone (Rytsk, 2020).

In summarizing the analysis of previously conducted reconstructions of the geodynamic history, it can be noted that within the studied territory, considering its location at the junction of structures of the Siberian Platform and the Central Asian Folded Belt, active processes of sedimentation, magmatism, metamorphic and metasomatic rock transformations, as well as intensive tectonic vertical and horizontal movements of crustal blocks at various depth levels, have occurred from the Archean to the present day. These phenomena were accompanied by the concentration, redistribution of mineral resources, and active ore formation. The formation of mineral deposits is associated with almost every stage of geological development (Mitrofanova et al., 2012).

From a metallogenic perspective, the territory belongs to the Sayan-Transbaikalian province and the Baikal-Patom mineragenic subprovince. Known ore occurrences are included in the Chuya-Tonod gold-rare metal-uranium-iron ore mineragenic zone (Makarev, Mironov, 2014). The most important mineral resources are gold and uranium (Fig. 1B). Tin deposits, as well as tungsten and beryllium, have secondary significance. Numerous occurrences of iron, titanium, and high-alumina raw materials are also known in the Riphean framing of the Tonoda and Chuya granitoid uplifts.

In the context of the results obtained in this study, it should be noted that the territory of the western part of the BPB is characterized by extremely complex tectonic structure. Faults with northeastern, northwestern, and less commonly near-latitudinal and submeridional orientations are widespread here. A predominance of northwestern vergence of the slip surfaces for faults of the main directions has been established, consistent with the vergence of folded structures, indicating their interrelationship. A widespread manifestation of polycyclic thrust dislocations in the junction zone between the Siberian Platform and the fold belt, and the presence of powerful dynamometamorphic zones are observed. Faults with northwestern orientation, despite clear expression in the relief, are poorly studied and identified mainly from geophysical and remote sensing data. As a result of field works and conducted geological mapping, northwestern faults are unambiguously identified as left-lateral strike-slips (Koveshnikov et al., 1989). Faults of sub-latitudinal orientation, according to researchers, were formed at the late stages of tectonic activation (Shmankevich et al., 1983). At the surface, these faults are manifested by large scarps and zones of intensive schistosity of rocks. According to data from previous studies (Ivanov et al., 1982), these faults are meso-deep, and the time of formation for most of them is attributed to the Early Proterozoic. The majority of all faults were repeatedly reactivated throughout the long geological history of the territory, leading to the formation of powerful zones of cataclasis, mylonitization, and schistosity of rocks (Makaryev et al., 2010; Mitrofanova et al., 2012). In many cases, the modern hydro-network inherits features and is determined by tectonics, which allows the use of structural-geomorphological analysis for reliable reconstruction of elements of the fault framework.

Materials and methods

The identification of lineaments within the studied territory, in contrast to most works implementing lineament analysis, was conducted not using satellite imagery but by visualizing and analyzing a Digital Elevation Model (DEM) (Ustinov, Petrov, 2016; Minaev et al., 2024a; Minaev et al., 2024b; Ustinov et al., 2024a). This approach takes into account the close connection of the term "lineament" with morphological features of the relief and the results of the authors' research for other territories based on this method. Considering the possibilities of artificial computer scaling of the Earth's surface and the variety of tools for its visualization, this method is effective even in areas with weakly dissected relief. The DEM of the territory was visualized in a Geographic Information System (GIS) environment using open and filtered (with anthropogenic objects and forests removed) FABDEM (Forest And Buildings removed Digital Elevation Model) data with an original spatial resolution of ≈30 meters per pixel. This DEM was created based on global radar interferometric survey data from COPDEM-30 (Copernicus DEM) (Hawker et al., 2022). The survey results are provided as raster images with elevation values for each pixel in GeoTIFF format, containing georeferencing metadata (Fig. 2A). Subsequently, using GIS tools, the DEM can be visualized, for example, as a hillshade map, to achieve the best results for lineament identification (Fig. 2B). Lineaments were automatically extracted from the

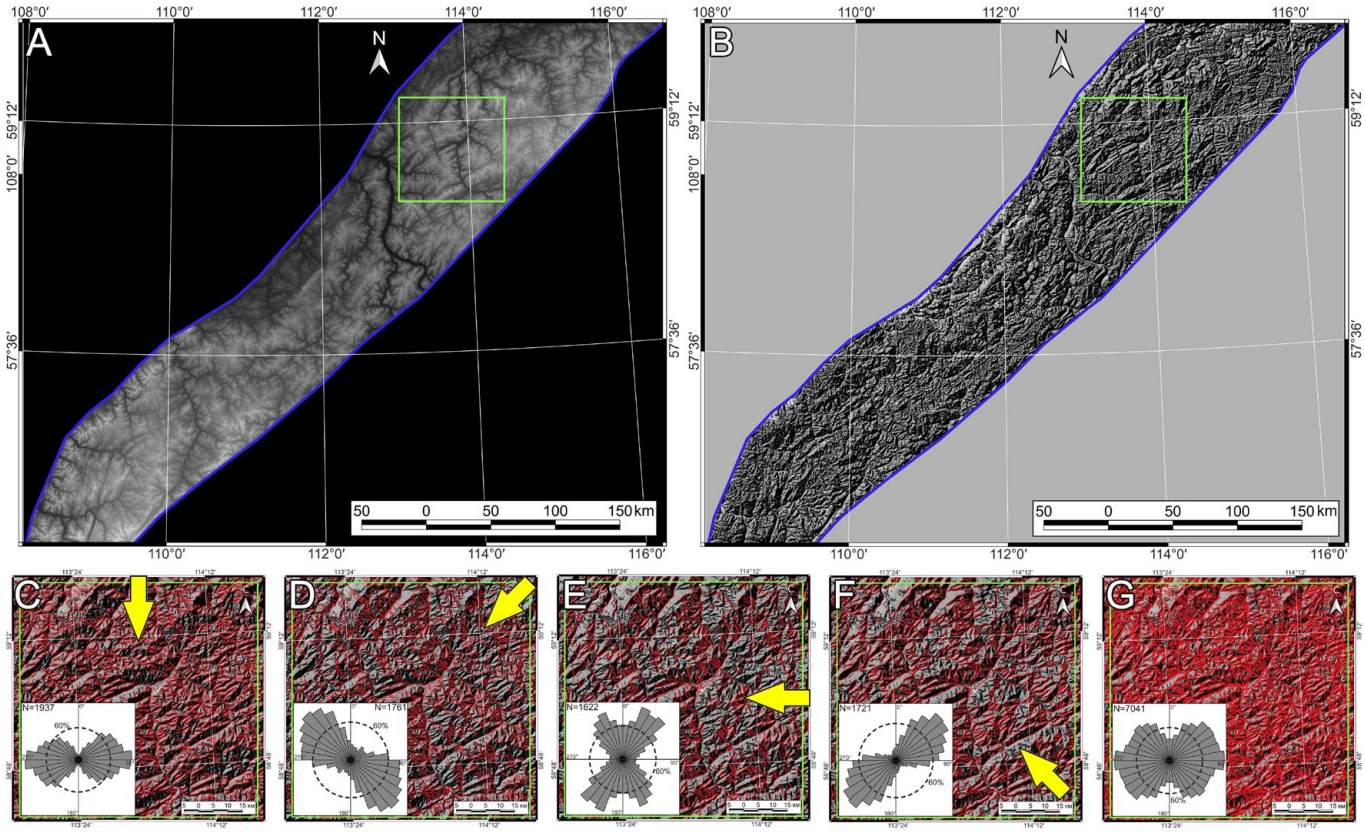

Fig. 2. Scheme of the sequence of automatic lineament identification using the developed software based on neural network technologies (Grishkov et al., 2023): A – initial data of the digital elevation model (DEM) FABDEM for the studied territory in GeoTIFF format; B – visualized DEM as a hillshade map; C–F – results of filtering a fragment of the territory's DEM with visualization as a hillshade map in four main directions (shown by yellow arrow): N–S (C), NE–SW (D), E–W (E), SE–NW (F) with identified lineaments (red lines) and rose diagrams of their orientations; G – total result of lineament identification in all directions of DEM filtering with its visualization on a hillshade map.

DEM using software developed with the participation of some of the article's authors, employing neural network technologies (Grishkov et al., 2023). This allowed for the automatic identification of linear structures in the way an expert operator would solve the task.

Before the lineament identification procedure, to optimize their extraction using automatic software tools, a method of nonlinear directional filtering of the DEM was applied. This allowed for the enhancement of all morphostructural features of the territory at possible positions of the light source. Directional filtering, in accordance with well-known methodologies (Paplinski, 1998; Suzen, Toprak, 1998; Enoh et al., 2021), was performed in four main directions: N–S (0°), NE–SW (45°), E–W (90°), and SE–NW (135°). Corresponding hillshade maps were generated for each direction, and lineaments were extracted from each using the developed software (Fig. 2C-E). Subsequently, the extracted linear elements were combined into a single layer, reflecting all possible lineaments at the considered level of DEM generalization based on the structural features of the relief (Fig. 2G).

The applied approach, taking into account the relatively high initial spatial resolution of the used DEM (≈ 30 meters per pixel), allows for the identification of numerous lineaments within the territory. These lineaments may reflect relatively short fault structures of the lowest ranks (at the scale of the studied area), characterizing the most local level compared to other structures forming the overall tectonic framework. These linear elements can be interpreted as so-called "megacracks" feathering extensive major faults (Petrov et al., 2010; Rebetsky et al., 2017).

To solve the problem of identifying extensive, high-rank faults that are marked by longer lineaments, as well as identifying all linear relief features expressed at various scale levels, it was proposed to artificially "degrade" the spatial resolution of the original DEM with a specific step. For each degraded resolution level, the procedures of DEM filtering in four directions and automatic lineament extraction are repeated. The step for reducing the DEM image spatial resolution was determined empirically, considering minimal data loss and the elimination of duplicate linear objects belonging by geometric parameters to the same rank. This allowed for the extraction of lineaments of various lengths, reflecting fault structures of different ranks, and thereby enabled the consideration of the scale effect in

the development of the fault framework elements of the territory during subsequent tectonophysical analysis (Petrov et al., 2017; Petrov et al., 2019).

The orientations of the identified lineaments and their spatial distribution are usually demonstrated for clarity using rose-diagrams and relative density maps. Rose-diagrams, created in this study, unlike the most structural-tectonic studies, demonstrate not only the number of linear objects with different azimuths, but also their extent, which allowed displaying the lengths of rays on rose-diagrams proportionally to the sum of lengths of linear objects of the considered azimuth intervals. Such systematic approach makes it possible to assess the prominence of specific generations of linear structures within the study area and to indirectly compare the magnitudes of deformation from different stages.

Relative specific density maps of lineaments demonstrate their quantity, taking length per unit area into account. The main parameters for constructing these maps in a GIS are the pixel size and the search radius, which by default should always be larger than the pixel size. The value in each pixel of the density map represents the ratio of the total length of linear objects within a circle, determined by the search radius, to the area of that circle. In this case, only lines or their parts that are exclusively inside the circle are taken into account (Fig. 3). The method of calculating relative density of lineaments using circles is chosen to minimize edge effects and ensure uniform coverage of the area. The percentage of circle overlap was set to 20%, which allowed to maintain smooth transitions between density values. In accordance with the determined DEM generalization step for which the lineament extraction procedure was conducted, the aforementioned parameters vary depending on the number of extracted linear objects, gradually increasing from the local to the

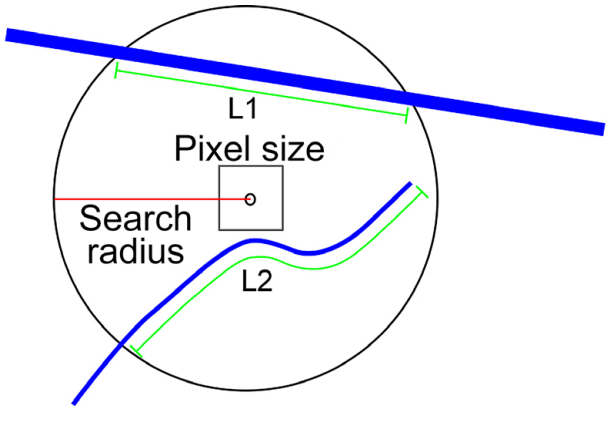

Fig. 3. Algorithm for creating a relative specific density map of linear objects in a GIS: blue lines represent linear objects; green lines represent segments of linear objects within the search radius (circles); L1 and L2 – of the linear object segments within the search radius used in calculating the density value for the designated pixel.

supra-regional level. The step for increasing parameters to construct relative specific density maps was also determined empirically but in direct dependence on the DEM generalization step.

In addition to the lack of consideration for the scale effect in the development of the fault systems framework when implementing lineament analysis, researchers in the context of forecasting the localization of mineral resources associated with fault structures often consider all lineaments marking fault zones as prospective areas for discovering ore mineralization. This approach is fundamentally incorrect, since systems of multi-scale fault structures, belonging to various genetic (kinematic) types, are formed during specific stages of tectogenesis and depend on the parameters of the stress-strain state (SSS) that prevailed during their formation. Depending on their kinematic type, fault structures can exist in various tectonophysical settings – from compression to extension – which significantly influenced the potential for fluid migration and the deposition of rich ore mineralization. Consequently, to reconstruct these settings, it is crucial to identify the type of each structure. This can be done only taking into account tectonophysical models of fault zone formation.

In this regard, it is important to note that, according to E.M. Anderson's theory of fault formation, three main types of faults are identified: normal, strike-slips and reverse faults (Anderson, 1905). At the same time, using physical-mechanical experiments and models, two main mechanisms of rock destruction are proven: tension and shear. The last one can be longitudinal and transverse (Kocharyan, 2021). Strike-slip movements, especially along extensive faults, can be reliably established using classical structural methods by proving block displacement along the fracture plane (Kuzmin, 2018). Considering the geodynamic development features of the studied territory reconstructed by predecessors – the manifestation of accretionary-collisional processes involving the attachment of BFA terranes to the Siberian Craton in a north-western direction – it is possible to assume a predominantly strike-slip nature of deformation during the formation of extensive supra-regional fault structures. Obviously, this stage of the geological history of the territory was one of the most powerful tectonic events that has been universally reflected in the relief. Subsequently, according to various estimates, one to three Early Paleozoic tectono-magmatic activation stages took place. During these stages, it is most likely that new structures did not form, but rather there was repeated reactivation of previously established faults (Mitrofanova et al., 2012).

At some distance in both directions from the strike-slip plane, a structurally weakened zone is usually observed. This zone is characterized by a higher density of cracks (fractures) compared to the surrounding rock

mass, which decreases exponentially with distance from the axis (fault plane) of the main fracture (Rats, Chernyshev, 1970; Faulkner et al., 2011). Such areas are termed the "zone of dynamic influence of the fault" or "damage zone of the fault" (Sherman et al., 1983; Sherman, 2014). Model experiments conducted under the guidance of K.Zh. Seminsky have shown that this zone is most often extremely heterogeneous. Within its structure, it is possible to distinguish subzones of intense fracturing (under conditions of local extension – transtension) and subzones of reduced fracturing (under conditions of local compression – transpression). Among other things, the width and properties of fault zones vary significantly with depth due to increasing mean pressure and temperature, as well as along strike due to the complex geometry of the fault (Anders, Wiltschko, 1994; Wilson et al., 2003; Faulkner et al., 2018).

Based on the above, and considering the decisive role of shear deformations in the process of fluid migration and ore deposition, various tectonophysical models for the formation of crack paragenesis within extensive (major) strike-slip fault zone were considered to reconstruct the conditions under which the identified multi-rank structures existed during a specific stage of tectogenesis (Riedel, 1929; Gzovsky, 1975; Smirnov, 1976; Hancock, 1985). P.L. Hancock presents the most comprehensive summary scheme of sets of primary and secondary feathering structures observed in shear zones both prior to and after the formation of a major fault (Hancock, 1985) (Fig. 4).

This model, as the most comprehensive, was used in our study to interpret the identified lineaments for reconstructing the parameters of shear-related SSS at various levels of DEM generalization. To automate the process of classifying linear objects of different ranks based on the P.L. Hancock model, the proprietary software "Lineament Stress Calculator" (LSC), developed by A.D. Svecherevsky, was applied. This software has proven highly effective in numerous studies by the article's authors for reconstructing strike-slip tectonic stresses using the identified lineament network within fault zones (Minaev et al., 2024a; Minaev et al., 2024b; Ustinov et al., 2024a).

After calculating the SSS parameters that acted during a specific stage of tectogenesis, it is important to visualize segments of the identified fault structures of different kinematic types with the greatest degree of opening and high permeability values. This task can be solved based on calculating the slip tendency coefficient (μ), which allows for a quantitative assessment of zones of deformation concentration and dispersal along the strike of the assumed fault structure (Fig. 5). The coefficient μ is defined as the ratio of shear (τ) to effective (σ_n) normal stresses (Fuchs, Müller, 2001):

$$\mu = \frac{\tau}{\sigma_n}.$$

Shear and effective stresses can be calculated by formulas (Jaeger, Cook, 1979):

$$\tau = \frac{S_1 - S_3}{2} \sin 2\phi,$$

$$\sigma_n = \frac{S_1 + S_3 - P_f}{2} + \frac{S_1 - S_3}{2} \cos 2\phi,$$

where S_1 – stress value along the axis of maximum compression, S_3 – stress value along the axis of minimum compression, P_f – fluid pressure, ϕ – angle between the

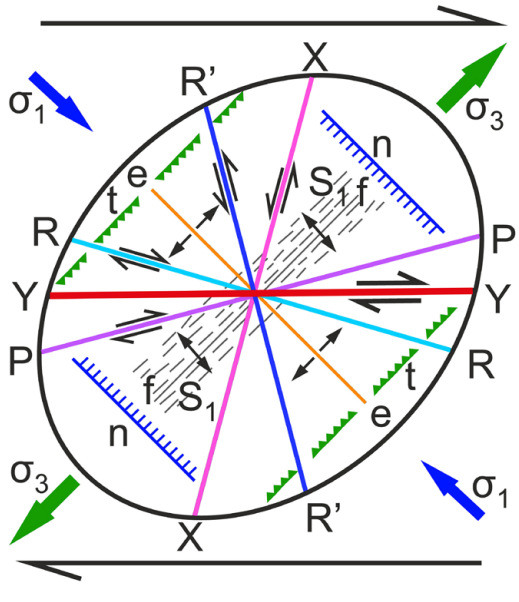

Fig. 4. Paragenesis of structural elements forming in a strike-slip fault zone under simple shear, after (Hancock, 1985), on the example of a right-lateral strike-slip: Y (red) – major strike-slip faults; R (light blue) and R' (blue) – conjugate primary strike-slips; X (pink) and P (violet) – secondary strike-slips; e (orange) – tension fractures; n (blue) – normal faults; t (green) – reverse faults; f – folds; S_1 – cleavage; arrows indicate: σ_1 (blue) – maximum compression axis, σ_3 (green) – maximum extension axis.

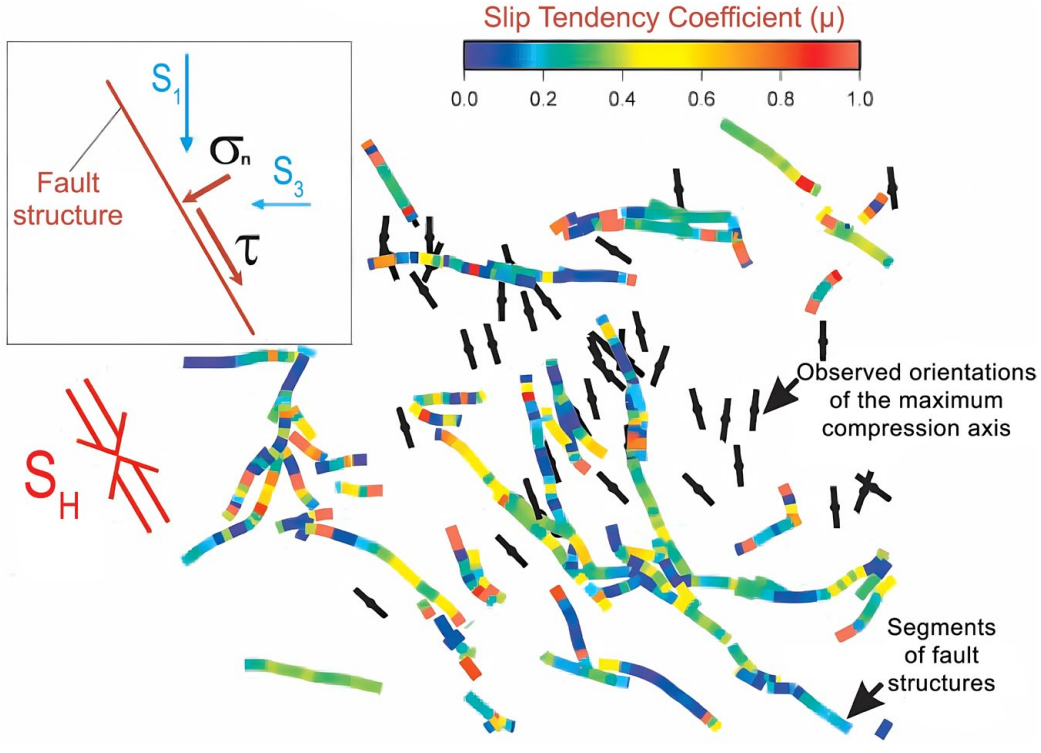

Fig. 5. General scheme for determining the slip tendency coefficient (μ) based on the combination of orientations of regional anisotropic stresses (black symbols – orientation of the maximum compression axis) with orientations of segments of fault structures, with calculation of the ratio of shear stress (τ) to normal stress (σ_n) for fault segments (Fuchs, Müller, 2001): S_1 – axis of maximum compression, S_2 – axis of minimum compression, S_H – orientation of the regional maximum compression axis. Segments demonstrating the greatest degree of hydraulic activity are shown in yellow and orange.

normal to the fault plane and the axis of S_1 stress action.

It has been proven that the most hydraulically active segments of fault structures possess $\mu \approx 0.6$ (Jaeger, Cook, 1979; Fuchs, Müller, 2001).

Unfortunately, for conducting calculations in accordance with the given formulas, there is no reliable information on the magnitudes of stresses and fluid pressure for a certain stage of tectogenesis and the associated geodynamic settings of lithosphere development. However, it is known that the formation of an extensive supra-regional strike-slip fault, reflecting collisional-accretionary processes, requires a significant difference between the values of S_1 and S_3, with $S_1 > S_3$ (Zoback, 2018). Considering this, the values of S_1 and S_3 are conventionally assumed to be 70 MPa and 20 MPa, respectively. In this case, shear stresses at established values of the angle (φ) between the normal to the fault plane and the axis of S_1 stress reach 25 MPa, which corresponds to the average values of tangential stresses for modern settings of intraplate orogenesis and boundaries of lithospheric plates (Rebetsky et al., 2009). In addition, at such S_1 and S_3 values for the used sample of objects, the calculated values of the slip tendency coefficient range from 0 to 0.67. This significantly simplifies further classification of segments of fault structures by permeability values. Taking into account that fault structure segments show a smooth decrease in hydraulic activity as the coefficient decreases, segments with μ in the range from 0.45 to 0.67 are defined as hydraulically active for further visualization. Fluid pressure values were not taken into account, since they do not have a significant influence on the final result. According to model calculations by Yu.L. Rebetsky, fluid pressure differs from lithostatic for modern areas of intraplate orogenesis by 0.6 – 0.8 times (Rebetsky, 2008).

Within the multi-scale approach, lineament identification and their tectonophysical interpretation is carried out. This allows to determine the parameters of the SSS characteristic of a certain stage of tectogenesis and, under the established geodynamic conditions, to visualize the most hydraulically active segments of faults based on calculating the slip tendency coefficient. The result is comprehensive structural-tectonophysical PM of localization of ore mineralization, which are presented in the form of visual schemes.

Among the variety of approaches to predictive modeling, one of the most effective and widely used methods in metallogenic mapping, mineral resources prospectivity analysis, and exploration has been applied to visualize the main tectonophysical criteria for ore mineralization localization in relation to the identified multi-rank fault zones, considering their kinematics. This method is the creation of a weighted PM (Franca-Rocha et al., 2003; Carranza, 2004; Porwal et al.,

2010; Shahi, Rouhani, 2014). These models are based on statistical algorithms that allow determining the conditional probability of the presence of an object in a specific section of the Earth's surface based on spatially visualized criteria and their correlation with already known (reference) ore objects.

The main principle of creating weighted PM is the identification of factors (criteria), which in this study are determined by the level of hydraulic activity of segments of discontinuous structures at a certain stage of tectogenesis and have the greatest significance for mineral concentration. After identifying significant spatial criteria, statistical analysis is performed to assess the influence of each on the presence of known ore occurrences – this determines the values of the weighting coefficients. These data are then combined into a single model that allows determining the conditional probability of the presence of an ore object in a specific section of the Earth's surface. Weighted PM are extremely effective prediction tools, as they allow combining heterogeneous types of data (geological, geochemical, geophysical, and others) and identifying hidden connections between them (Gitis et al., 2013). This is achieved through the normalization procedure, that is, bringing the scale of values of spatial criteria, which are heterogeneous data in various intervals differing from each other sometimes by orders of magnitude, to values from 0 to 1 for their correct comparison and integration into the final model.

Results

The identification of lineaments through sequential degradation of the DEM spatial resolution allowed for highlighting the evolutionary features of the multi-rank fault structure framework in the horizontal plane, from local to supra-regional levels, considering the study area. Obviously, with such approach, the number of extracted objects decreases while the average lineament length increases. For studied extensive territory, these parameters range from 382,866 objects with an average length of 616 meters at the most local level, to 254 objects with an average length of 19,127 meters at the established supra-regional level (Fig. 6). The generalization step from the original DEM spatial resolution (30 meters per pixel) is constant and constitutes a factor of 2 (60 meters per pixel), 4 (120 meters per pixel), 6 (180 meters per pixel), 8 (240 meters per pixel), and so on, up to a degradation factor of 30 (900 meters per pixel) (No. 1–16 in Fig. 6). Subsequently, based on the analysis of rose diagrams showing the orientations of the extracted lineaments, and taking into account the separation of a single system

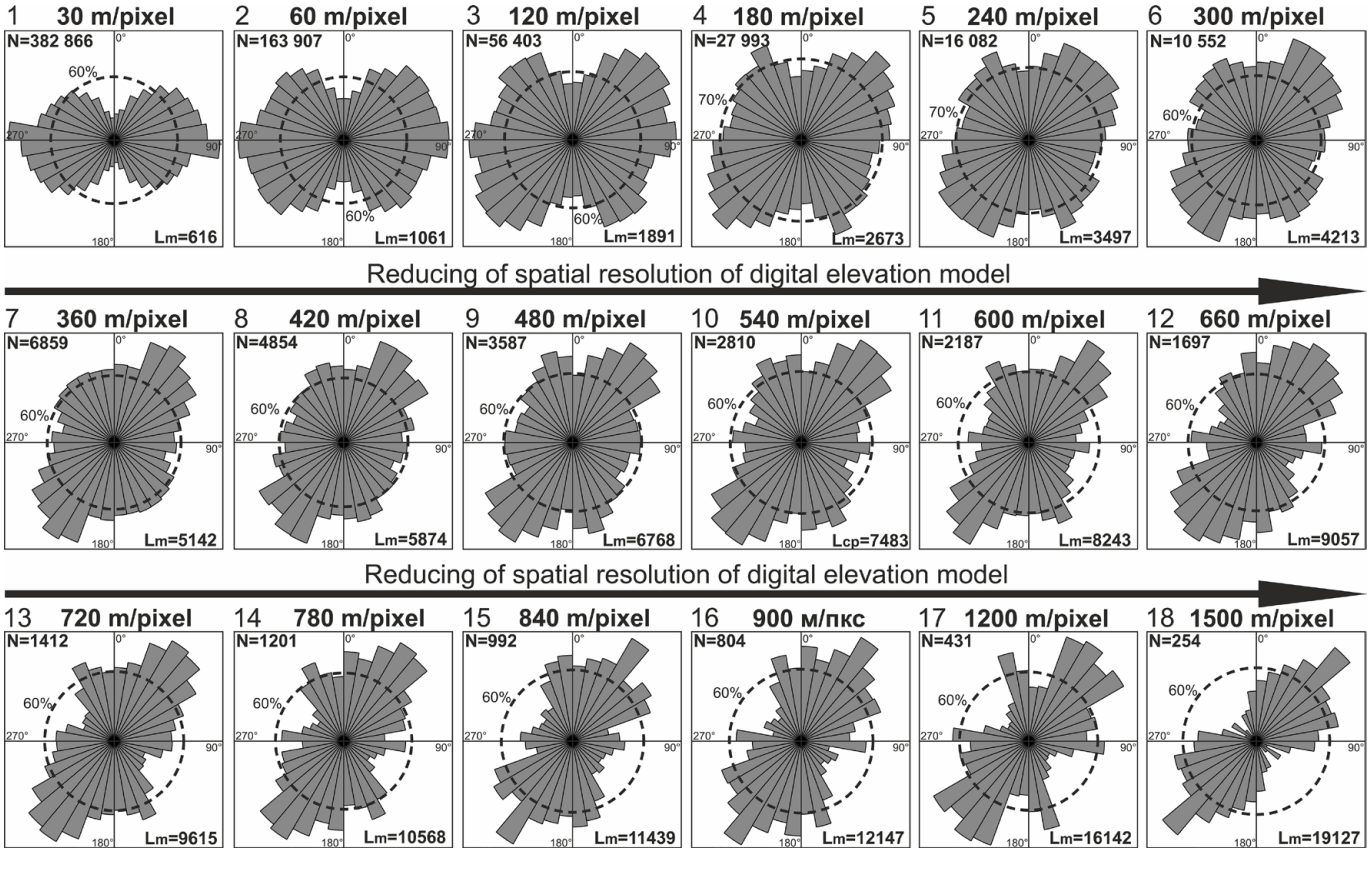

Fig. 6. Rose-diagrams of strike azimuths, taking into account lengths, number, and average length of automatically identified lineaments at each step of sequential artificial degradation of the spatial resolution of the DEM (No. 1–18): N – number of identified lineaments (rectilinear segments); Lm – mean length of identified straight-line segments of lineaments in meters; m/pixel – spatial resolution of the DEM in meters per pixel.

of structures, a conclusion about the final transition to the supra-regional scale level was drawn. To verify this conclusion, the results of lineament identification for DEMs whose spatial resolution is degraded in 40 (1200 meters per pixel) and 50 (1500 meters per pixel) times were added (No. 17, 18 in Fig. 6). Further degradation of the DEM spatial resolution is not meaningful, as the number of extracted linear objects within the study area becomes critically small for statistical processing and tectonophysical interpretation.

Figure 6 demonstrates that at the most local levels the sub-latitudinal generation of structures developed with some scatter in orientations from it of less extensive lineaments, probably marking systems of megacracks feathering the main structural trend (No. 1–2 in Fig. 6). When transitioning to lower scale levels, a gradual disappearance of sub-latitudinal and ubiquitous development of northwestern and northeastern systems of lineaments is observed (No. 3–6 in Fig. 6). At more regional levels of DEM generalization, the system of northeastern strike receives maximum development, which is sub-parallel to the boundary of the BFA and the Siberian platform (No. 7–18 in Fig. 6). Most likely, along extensive fractures of this system, the main strike-slip deformations occurred within accretion-collision processes. Furthermore, in addition to the main northeastern generation of supra-regional faults, less pronounced systems with north-northwest and sub-meridional strikes are traceable on the rose diagrams of high scale levels. For their classification and determination of kinematic type, it is necessary to conduct tectonophysical interpretation of the paragenesis of all structures in the main strike-slip zone.

Relative specific density maps of the extracted lineaments of various ranks (taking into account average length and quantity), constructed at various empirically selected parameters of pixel size and search radius depending on the DEM generalization level, demonstrate a heterogeneous spatial distribution of objects during preliminary visual analysis (Fig. 7). The maps use a color

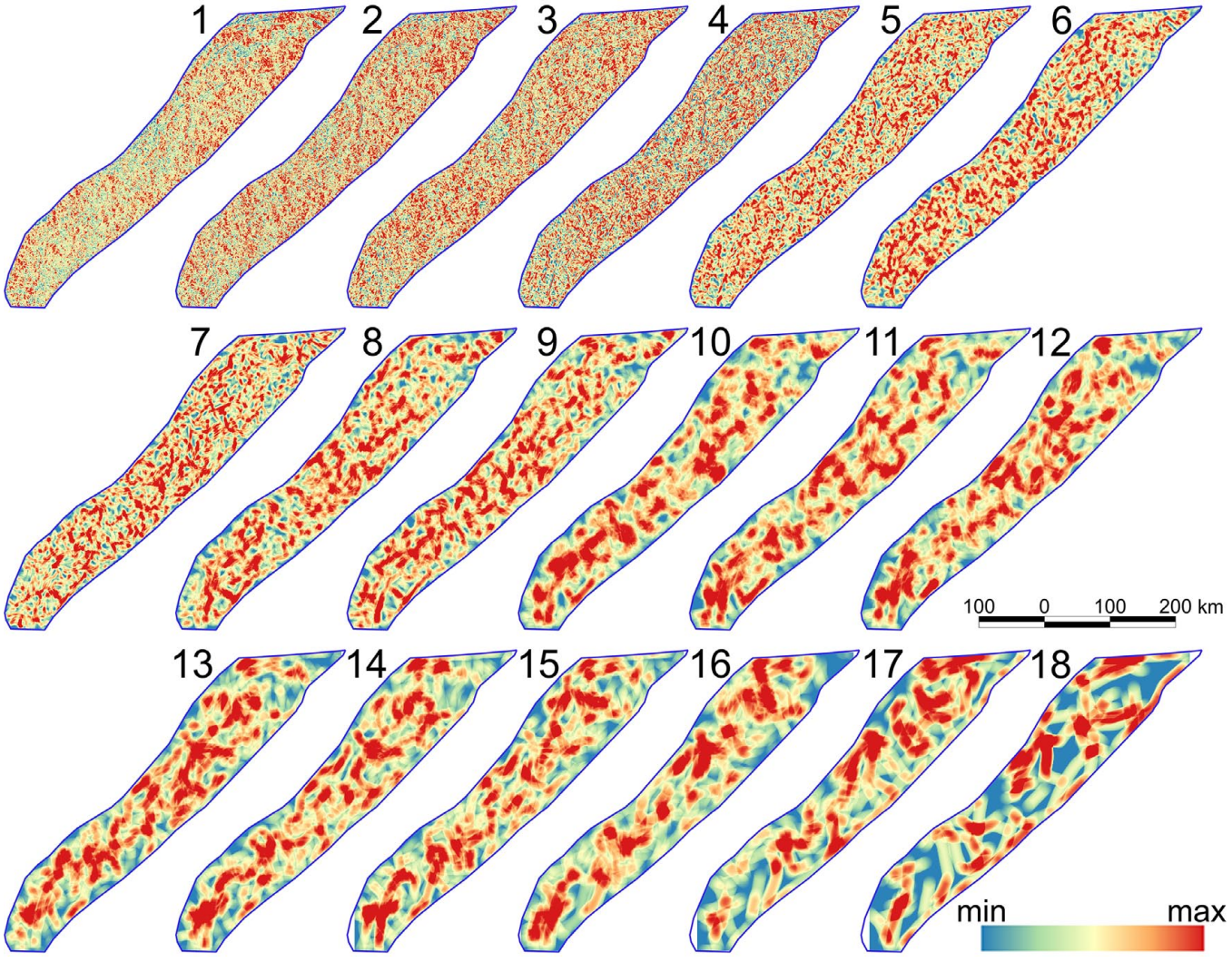

Fig. 7. Relative specific density maps for lineaments extracted at different scale levels of DEM generalization (No. 1–18): 1 – 30 m/pixel; 2 – 60 m/pixel; 3 – 120 m/pixel; 4 – 180 m/pixel; 5 – 240 m/pixel; 6 – 300 m/pixel; 7 – 360 m/pixel; 8 – 420 m/pixel; 9 – 480 m/pixel; 10 – 540 m/pixel; 11 – 600 m/pixel; 12 – 660 m/pixel; 13 – 720 m/pixel; 14 – 780 m/pixel; 15 – 840 m/pixel; 16 – 900 m/pixel; 17 – 1200 m/pixel; 18 – 1500 m/pixel.

scale from blue to red to indicate areas from minimum to maximum density of linear objects, indirectly reflecting manifestations of deformations of various intensities.

In order to identify objective and closer relationships between the densities of lineaments identified at various levels of DEM generalization, a correlation analysis for raster images of created maps of relative specific density of lineaments was conducted (Table 1).

Even taking into account the fact that schemes of relative specific density of lineaments were created at various parameters of pixel values and search radius, a stable correlation dependence is observed between the compared rasters. This allows for a more definitely attributing of the extracted multi-rank lineaments and the fault structures marked by them to a specific scale level. Thus, density maps constructed for lineaments extracted using DEMs with spatial resolutions of 30, 60, 120, 180, 240, 300, 360, and 420 meters per pixel (Nos. 1–8 in Table 1 and Figs. 6, 7) demonstrate strong correlation and can be attributed to the local scale level. Density maps from 9 to 14 in Table 1 and Figures 6 and 7, corresponding to lineaments extracted using DEMs with spatial resolutions of 480, 540, 600, 660, 720, and 780 meters per pixel, respectively, also demonstrate strong correlation among themselves, which allows attributing them to the next scale level – regional. At the same time, the rasters of lineament density maps of local and regional scale show a moderate correlation strength with each other, indicating a certain degree of their interconnection and structural inheritance. Upon transitioning to supra-regional levels, the created density maps 15 and 16 in Table 1 and Figures 6 and 7 for lineaments identified by DEMs with spatial resolutions of 840 and 900 meters per pixel are characterized by weak correlation both among themselves and relative to other, more local levels. The highest scale levels (No. 17, 18 in Table 1 and in Fig. 6, 7) for lineaments identified using DEM with spatial resolution 1200 and 1500 meters per pixel, demonstrate an absence of correlative relationships with all other levels, while showing an extremely weak correlation between themselves. The high-level of lineament identification probably reflect the development of individual supra-regional fault structures of varying lengths that played the role of accretionary sutures and inter-block boundaries, which is confirmed by the absence or presence of weak correlation

	Local scale level								Regional scale level						Supra-regional scale level			
No.	**1**	**2**	**3**	**4**	**5**	**6**	**7**	**8**	**9**	**10**	**11**	**12**	**13**	**14**	**15**	**16**	**17**	**18**
1	1.00	0.97	0.88	0.88	0.92	0.88	0.87	0.80	0.77	0.65	0.65	0.67	0.66	0.67	0.53	0.50	0.09	0.03
2	0.97	1.00	0.91	0.88	0.89	0.87	0.86	0.80	0.78	0.66	0.65	0.66	0.66	0.67	0.52	0.50	0.10	0.03
3	0.88	0.91	1.00	0.85	0.81	0.80	0.79	0.77	0.77	0.67	0.67	0.64	0.67	0.66	0.51	0.49	0.09	0.03
4	0.88	0.88	0.85	1.00	0.84	0.81	0.81	0.75	0.76	0.62	0.61	0.63	0.62	0.64	0.50	0.49	0.10	0.03
5	0.92	0.89	0.81	0.84	1.00	0.89	0.90	0.82	0.76	0.64	0.63	0.67	0.65	0.67	0.53	0.51	0.09	0.03
6	0.88	0.87	0.80	0.81	0.89	1.00	0.99	0.79	0.73	0.62	0.61	0.65	0.63	0.65	0.51	0.49	0.08	0.03
7	0.87	0.86	0.79	0.81	0.90	0.99	1.00	0.79	0.74	0.63	0.61	0.65	0.63	0.65	0.51	0.50	0.08	0.03
8	0.80	0.80	0.77	0.75	0.82	0.79	0.79	1.00	0.79	0.62	0.61	0.63	0.62	0.63	0.50	0.43	0.13	0.04
9	0.77	0.78	0.77	0.76	0.76	0.73	0.74	0.79	1.00	0.84	0.83	0.84	0.84	0.84	0.50	0.53	0.08	0.03
10	0.65	0.66	0.67	0.62	0.64	0.62	0.63	0.62	0.84	1.00	0.87	0.86	0.86	0.85	0.54	0.43	0.05	0.03
11	0.65	0.65	0.67	0.61	0.63	0.61	0.61	0.61	0.83	0.87	1.00	0.86	0.84	0.85	0.53	0.43	0.05	0.03
12	0.67	0.66	0.64	0.63	0.67	0.65	0.65	0.63	0.84	0.86	0.86	1.00	0.86	0.83	0.57	0.48	0.05	0.03
13	0.66	0.66	0.67	0.62	0.65	0.63	0.63	0.62	0.84	0.86	0.84	0.86	1.00	0.85	0.55	0.44	0.05	0.03
14	0.67	0.67	0.66	0.64	0.67	0.65	0.65	0.63	0.84	0.85	0.85	0.83	0.85	1.00	0.58	0.48	0.07	0.03
15	0.53	0.52	0.51	0.50	0.53	0.51	0.51	0.50	0.50	0.54	0.53	0.57	0.55	0.58	1.00	0.59	0.05	0.07
16	0.50	0.50	0.49	0.49	0.51	0.49	0.50	0.43	0.53	0.43	0.43	0.48	0.44	0.48	0.59	1.00	0.05	0.04
17	0.09	0.10	0.09	0.10	0.09	0.08	0.08	0.13	0.08	0.05	0.05	0.05	0.05	0.07	0.05	0.05	1.00	0.28
18	0.03	0.03	0.03	0.03	0.03	0.03	0.03	0.04	0.03	0.03	0.03	0.03	0.03	0.03	0.07	0.04	0.28	1.00

Table 1. Correlation coefficient between relative specific density maps for lineaments extracted at different scale levels of DEM generalization (numbers correspond to Figs. 6, 7). Colors: dark green – strong correlation; bright green – medium correlation; light-green – weak correlation; pink – extremely weak correlation; white – no correlation.

connections among themselves and with structures of lower ranks.

The next important step, in the context of forecasting ore mineralization and reconstructing the geodynamic evolution of the territory based on structural-geomorphological features, was the reconstruction of the orientations of the compression and extension axes within the shear-related stress-strain state (SSS), as well as the determination of the kinematic types of the assumed multi-rank fault structures in accordance with the P.L. Hancock model (Fig. 8). Since on all rose diagrams from supra-regional to local (except the most local) scale levels, the system of northeastern strike is unambiguously the main structural trend (Fig. 6). Then during the interpretation structures of this generation were considered as major faults. In this case, the compression axes show east-northeastern and sublatitudinal orientations (No. 3–18 in Fig. 8). The extension axis is orthogonal to these directions. Furthermore, the northeastern supra-regional faults themselves are right-lateral strike-slips. This situation most likely corresponds to the established settings of oblique accretion of the BFA terranes to the Siberian craton during the period of accretionary-collisional processes.

The next, less extensive fault system, manifested exclusively at high regional and supra-regional scale levels (No. 11, 13–17 in Fig. 8), is a generation of structures with north-northwestern strike. Taking into account that the orientation of these faults, in accordance with the applied shear deformation model, coincides with the orientation of the extension axis, it is logical to assume that they form reverse faults. The presence of extensive regional reverse faults of these orientations within the considered territory has been noted by many researchers and taken into account in constructing geological maps (Ivanov et al., 1982).

At intermediate scale levels, among others, structures with northwestern orientation are prominently expressed (No. 3–6 in Fig. 8). According to the results of previous studies, these faults were identified exclusively based on geomorphological relief features and the interpretation of geophysical data. They also align well with the reconstructed parameters of the shear-related SSS and were formed as secondary (antithetic) left-lateral strike-slips relative to the major northeastern structures. A similar kinematic type for the considered structures was established as a result of field observations conducted earlier (Koveshnikov et al., 1989).

It is necessary to specifically note the tectonophysical reconstructions conducted for lineaments identified at the most local scale levels with DEM spatial resolution of 30 (initial resolution) and 60 meters per pixel (No. 1–2 in Fig. 8). As previously noted, a predominantly sub-latitudinal system of assumed fault structures is developed at these levels, with a slight scatter in angles from it of other, less pronounced, systems. The identified structures at these scale levels could, on the one hand, represent feathering megacracks for more extensive structures of higher ranks, while the trends of established extensive faults (northeastern and northwestern) might not manifest itself at the considered local level and, accordingly, not be reflected on rose-diagrams. On the other hand, they could form their own system of major strike-slip faults of a corresponding low rank, which acted during subsequent stages associated with tectonomagmatic activations of the territory. Therefore, for each of the indicated levels, additional reconstructions were conducted, where either the identified regional northeastern trend (No. 1b, 2b in Fig. 8) or the sublatitudinal structures (No. 1a, 2a in Fig. 8) were considered as the major structures. When considering the regional northeastern trend as the main fracture for these local levels, parameters similar to those established for regional and supra-regional levels were identified. They are characterized by east-northeastern orientation of the compression axis. The regional structures are right-lateral strike-slips, while sub-latitudinal trends were formed as antithetic primary shears (No. 1b, 2b in Fig. 8). When considering structures of sub-latitudinal orientation as major strike-slips for the two designated scale levels, different orientations of the principal SSS axes are revealed. At the most local level, during shear deformations, sublatitudinal fractures as main structures represent left-lateral strike-slips with northeastern orientation of the compression axis (No. 1a in Fig. 8). At the next, higher level, these fractures are right-lateral strike-slips with northwestern orientation of the compression axis (No. 2a in Fig. 8).

Taking into account the conducted reconstructions, it can be assumed that local sub-latitudinal faults at the initial stages were formed either as tension fractures or as primary antithetic shears in the zones of regional main northeastern accretionary sutures characterized by right-lateral slip. During subsequent stages of tectonomagmatic activation of the territory, the sub-latitudinal structures could have evolved first as left-lateral and then as right-lateral strike-slips due to an inversion of the stress-strain state (SSS) parameters. Consequently, these structures throughout the entire tectonic history recorded using the proposed approach (Late Precambrian – Early Paleozoic) were in the most favorable conditions for fluid migration. Most researchers also note the important role of faults of the considered orientation in the localization of ore mineralization, which is confirmed by the content of ore accumulations of most studied deposits in the area predominantly to relatively short faults of sub-latitudinal strike (Makarev et al., 2010; Mitrofanova et al., 2012; Ivanov et al., 1982; Shmankevich et al., 1983).

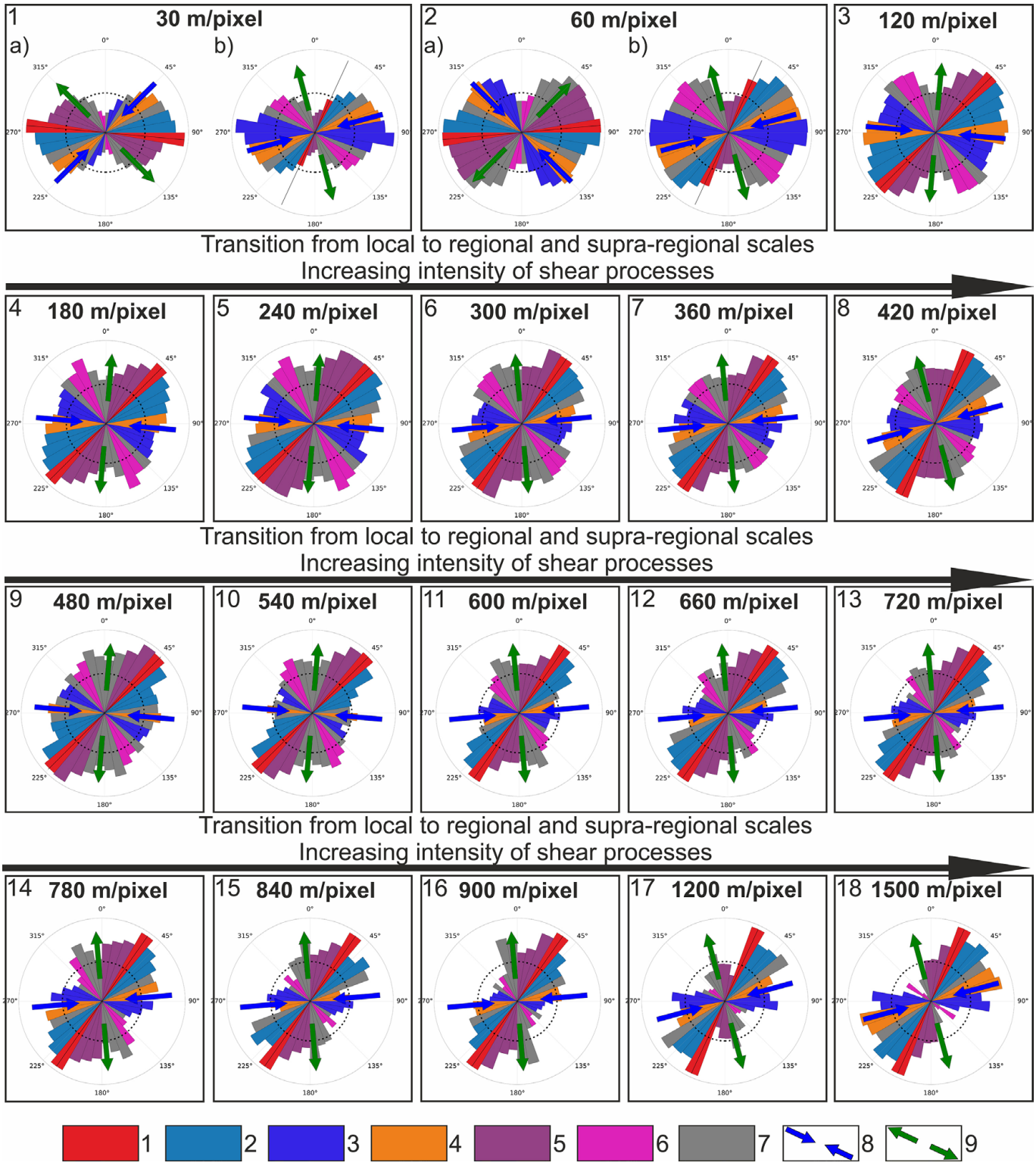

Fig. 8. Tectonophysical interpretation of the spatial position of lineaments identified at different levels of DEM generalization (No. 1–18), based on the P.L. Hancock's shear model using LSC software. 1 – major faults, 2 – primary synthetic strike-slips, 3 – primary antithetic strike-slips, 4 – tension fractures, 5 – secondary synthetic strike-slips, 6 – secondary antithetic strike-slips, 7 – unidentified lineaments, 8 – orientation of the axis of maximum compression, 9 – orientation of the axis of maximum extension. m/pixel – spatial resolution of the DEM in meters per pixel.

Summarizing the above, it is possible to identify the main, most manifested stages of tectogenesis within the studied territory.

I) The first stage is characterized by sub-latitudinal – east-northeastern orientation of the maximum compression axis, the position of which influenced the formation of the extensive regional and supra-regional major structures of northeastern strike functioned as right-lateral strike-slips. Also at this stage, the formation of regional reverse faults of north-northwestern and sub-meridional strikes occurs, in accordance with the maximum extension axis. Additionally, less extensive northwestern faults compared to the designated structures, as secondary antithetic shears with left-lateral strike-slip kinematics are formed. These SSS parameters are reconstructed for all assumed structures at every of the established scale levels and correspond to the most powerful strike-slip processes manifested ubiquitously within the considered area. These processes can be correlated exclusively with the established accretionary-collisional events of the attachment of BFA terranes to the Siberian craton, which took place at the end of the Late Precambrian (Gusev, Khain, 1995; Gordienko, 2006; Gordienko et al., 2013; Stanevich et al., 2007; Chugaev et al., 2018; Nikishin et al., 2010).

II) The second stage is most likely associated with tectonomagmatic activation of the territory in the Early Paleozoic and is occurred exclusively at the most local of the identified scale levels, which indicates a significantly lower intensity of deformations compared to the previous stage (at the scale of the studied area). The maximum compression axis was characterized by northeastern orientation, while sub-latitudinal faults farmed at the previous stage as tensions and primary antithetic shears underwent activation and functioned as left-lateral strike-slips with corresponding paragenesis of feathering megacracks of lower ranks.

III) The concluding stage is identified at a local scale level close to the previous one and is associated with further strike-slip movements along sub-latitudinal structures with inversion of SSS parameters. The sub-latitudinal faults acted as right-lateral strike-slips with northwestern orientation of the maximum compression axis. An additional criterion for attributing this stage to the concluding ones is the established as a result of geological mapping fact of the presence of relatively young local thrusts displacing ore bodies, which occurred in the northwestern direction towards the Siberian craton (Makarev et al., 2010; Mitrofanova et al., 2012). These thrusts could have formed under such reconstructed SSS parameters, specifically with a northeastern orientation of the maximum extension axis.

Based on the calculation of the slip tendency coefficient, taking into account the reconstructed orientations of the principal compression and extension axes, it is possible to visualize the most hydraulically active (conditionally permeable) segments of fault structures at the identified stages of tectogenesis. These stages, in terms of their intensity, encompass the established multi-scale structural-tectonic levels within the territory (Fig. 9).

The earliest of the reconstructed, the most powerfully manifested stage, , associated with accretionary-collisional processes and reconstructed for all scale levels, is characterized predominantly by northeastern and northwestern permeable structures (No. 1b, 2b, 3–18 in Fig. 9). The former represent right-lateral major strike-slips, while the latter are left-lateral primary and/or secondary antithetic shears. In Figure 9 only faults reflecting the maximum degree of shear deformation were considered in the calculations. It is important to note that tension structures, despite their much smaller number and significantly weaker manifestation within the area at regional and supra-regional scale levels – which is natural in accordance with laboratory shear experiments and known tectonophysical models – also possess a significant degree of opening and, accordingly, form permeable zones as well. At the first stage, these structures have sub-latitudinal orientations.

At the second and third stages, despite the reverse patterns in the orientations of the maximum compression and extension axes, the structures characterized by the highest permeability values were faults of sub-latitudinal and sub-meridional strikes (No. 1a, 2a in Fig. 9). It follows that supra-regional faults of northeastern orientation, whose influence is traced at all scale levels, could have acted as deep magma- and fluid-conducting structures, and consequently also as ore-conducting and possibly partially ore-hosting structures during the accretion of the BFA terranes to the Siberian craton. Meanwhile, according to the conducted reconstructions, the sublatitudinal structures initially formed as megacracks of tensile origin and later functioned as strike-slips in the process of further activations of the territory, being ore-localizing (ore-hosting).

The final outcome of the work was a comprehensive visualization of the results in a GIS in the form of maps showing areas with varying hydraulic activity at the established stages of tectogenesis. Such variation depends on the spatial position and proximity of fault structure segments with specific values of the slip tendency coefficient. The maps were compared with the locations of known (reference) ore occurrences. This task can be solved based on the creation of the relative specific density maps of linear objects, but in addition to pixel size and search radius, the weight value of each object determined by the value of the slip tendency coefficient was used.

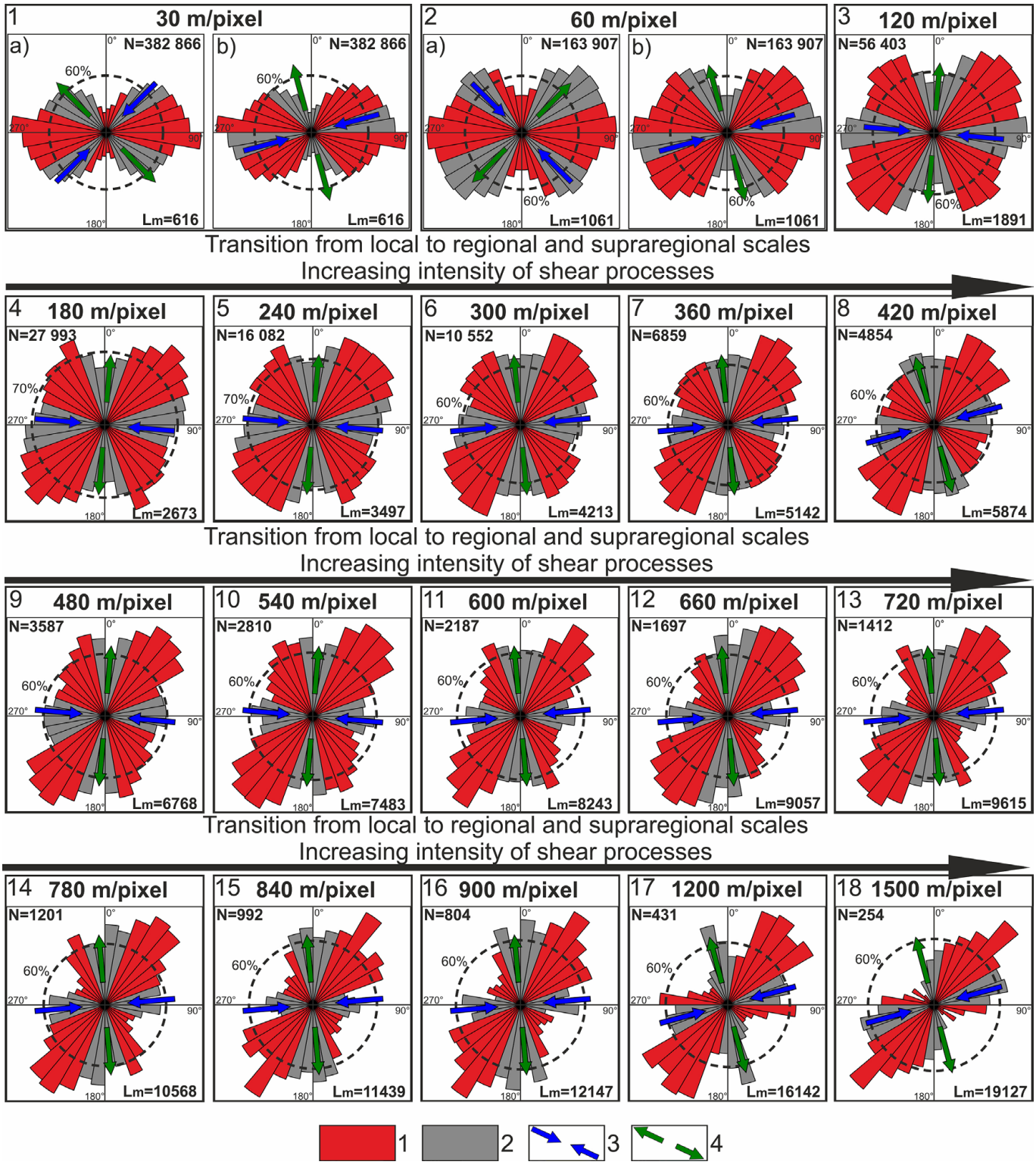

Fig. 9. Visualization based on rose-diagrams of orientations of hydraulically active segments of fault structures identified at different levels of DEM generalization, taking into account reconstructed SSS parameters (No. 1–18): 1 – conditionally hydraulically active segments of fault structures; 2 – conditionally impermeable segments of fault structures; 3 – orientation of the maximum compression axis; 4 – orientation of the maximum extension axis; N – number of identified lineaments (straight-line segments); Lm – mean length of identified lineaments in meters; m/pixel – spatial resolution of the DEM in meters per pixel.

This made it possible to assess the role of each scale level, stage, and their combined manifestation in the ore-forming process, and also served as the basis for creating comprehensive prospecting models (PM) for the considered territory (Fig. 10).

For the first stage of tectogenesis, in order to determine the role of multi-rank faults in the process of ore localization, taking into account the intensity of the processes reflected by it, models were created both separately for each of the scale groups of identified fault structures – the local, regional, and supra-regional levels (Fig. 10A–C and Table 1), and comprehensively for all groups combined (Fig. 10D).

The subsequent reconstructed stages differ by a much lower degree of tectonic manifestation and are recorded exclusively at separately taken steps of DEM generalization. Therefore, unified PMs were constructed for them, reflecting the distribution of permeable structures of the corresponding rank formed during the considered stage (Fig. 10D, E). A combined visualization and assessment of the joint influence of hydraulically active structures formed at various stages of tectogenesis – at the first and second (Fig. 10F), first and third (Fig. 10G) – were also performed. A combination of structures of the second and third stages of tectogenesis was attempted, but it did not yield a significant number of correlations with the location of reference ore objects, therefore it is not presented in Figure 10. In addition, PM of permeable structures that developed during all identified stages of tectogenesis was created (Fig. 10H).

A statistical comparison of the obtained maps with the position of known ore occurrences allowed for an assessment of the accuracy in percentages of the created PMs for each stage and scale level. The accuracy of models of structural permeability of faults formed at the first stage of tectogenesis decreases with increasing scale. At the local level it is 66%, at the regional level – 51%, and at the supra-regional level – 40% (Fig. 10A–C). This means that known ore occurrences tend to be more associated with areas where short, permeable structures of local levels converge, rather than those of regional or supra-regional levels. Despite this, the value of 66% is insufficiently significant for formulating further predictive assumptions about ore localization within the area. However, the comprehensive model of localization of permeable structures within the first stage of tectogenesis, covering all identified scale levels, demonstrates a higher value of 74% (Fig. 10D). It follows that the first stage of tectogenesis as a whole played both an ore-preparatory and an ore-localizing role. This was due to the development of paragenesis of multi-scale structures, where ore-bearing fluids migrated into near-surface areas along extensive deep-seated faults and were distributed in significantly less extensive feathering fractures against the background of accretionary-collisional processes.

PMs for the second and third stages of tectogenesis, associated with the predominant development of sub-latitudinal fractures identified at specific, exclusively the most local, scale levels, when compared with ore objects, received accuracy assessments of 61% and 55%, respectively (Fig. 10E, F). It can be concluded that these processes individually had a weak influence on ore localization within the area.

However, the created comprehensive models, which include a combination of the first and second stages (Fig. 10G), the first and third stages (Fig. 10H), and all three identified stages of tectogenesis (Fig. 10I), demonstrate assessed accuracy values of 94%, 75%, and 84%, respectively. It follows that the tectonic processes of the first and second stages had the most significant influence on ore localization. The third stage, as previously assumed, is most likely associated with the formation of thrusts in the northwestern direction towards the Siberian craton. This stage is younger and, most probably, played practically no role in the process of migration of ore-bearing fluids, merely causing some displacement of previously formed ore bodies. This is confirmed by the fact that for the comprehensive PM (Fig. 10I), reflecting all stages of tectogenesis, accounting for the strike-slip parameters of the third stage leads to a decrease in accuracy compared to the model including exclusively the strike-slip processes of the first and second stages of tectogenesis (Fig. 10G).

Discussion

Within the presented research, an approach for the sequential automatic identification of multi-rank lineaments, reflecting fault structures of various scale levels based on the use of a DEM, and their tectonophysical historical interpretation in the context of ore prediction has been formulated, developed, and presented for the first time. This interpretation is based on the permeability characteristics of fault segments, depending on the SSS parameters at a specific stage of tectogenesis and the kinematic type of each structure. The work was conducted for the extensive territory of the western part of the BPB, characterized by the most pronounced general features of tectonic development. Despite the obtained significant results, this approach may raise a number of questions among specialists that require clarification.

The lineaments identified based on the relief exactly coincide with faults established by ground surveys and displayed on the SGMs. This confirms the possibility of using morphological features of the territory's relief for reconstructing the framework of fault structures (Makarev et al., 2010; Mitrofanova et al., 2012).

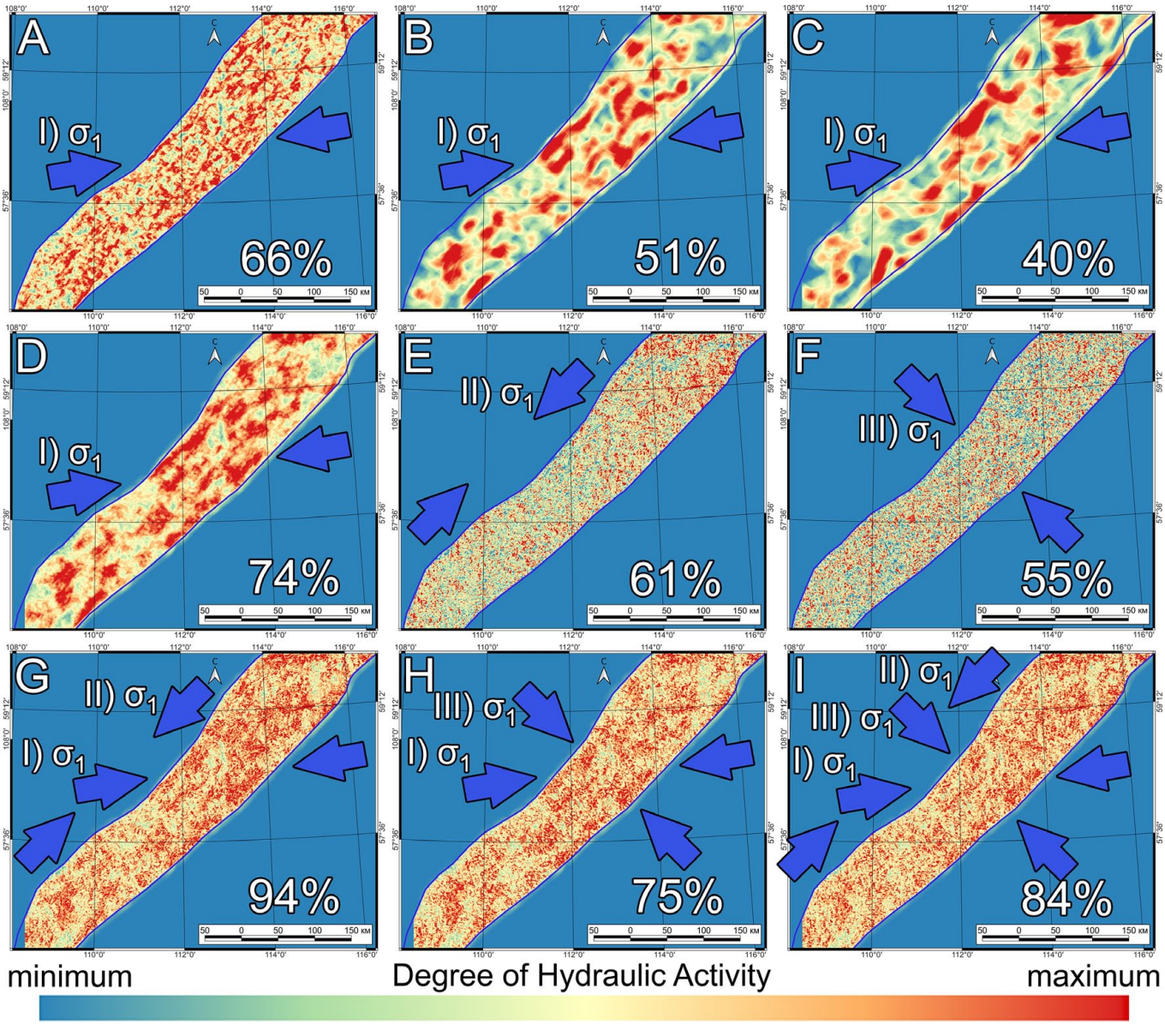

Fig. 10. Weighted prospecting models with an assessment of their accuracy, created based on visualization of hydraulically active segments of multi-scale fault structures, taking into account parameters of the identified stages of tectogenesis: A – fault structures of local scale level at the first stage of tectogenesis; B – fault structures of regional scale level at the first stage of tectogenesis; C – fault structures of supra-regional scale level at the first stage of tectogenesis; D – fault structures of all scale levels at the first stage of tectogenesis; E – fault structures of the corresponding local scale level at the second stage of tectogenesis; F – fault structures of the corresponding local scale level at the third stage of tectogenesis; G – fault structures at the first and second stages of tectogenesis; H – fault structures at the first and third stages of tectogenesis; I – fault structures of all identified stages of tectogenesis. Percentage values indicate the estimated model accuracy based on comparison with reference ore occurrences.

Many researchers also note the fact of inheritance of features of the tectonic structure of the region by the modern hydrographic network (Shmankevich et al., 1983). A comparison of rose-diagrams for established "ancient" faults and neotectonic fractures shows their almost complete overlap, which may indicate the constant reactivation (rejuvenation) of structures and their inheritance in the modern relief (Ustinov et al., 2024a).

With the applied approach, it is possible to establish the most global tectonic events in the geological history of the considered territory. Since this area remains seismically active to this day, there is no doubt that other fault structures reflecting modern stages of tectogenesis could develop as a result of seismic events. However, as the authors' field observation experience has shown, traces of these events are observed exclusively at local sites and do not contribute significantly to widespread changes in relief features established by ancient, incomparably more powerful processes over extensive areas.

Furthermore, for the tectonophysical interpretation of the identified multi-scale lineaments, exclusively the shear zone model (Hancock, 1985) was used, where the assumed major, most extensive structures by default represent strike-slips. Undoubtedly, the authors understand that in natural conditions, other various deformation mechanisms and their combinations may occur, such as normal faulting, reverse faulting, reverse strike-slips, normal strike-slips, thrust faulting, etc. However, longitudinal strike-slip, in contrast to transverse, which is more responsible for vertical movements of blocks, can be easily established in the horizontal plane based on geomorphological signs of block displacement and the analysis of the paragenesis of assumed feathering megacracks relative to the major structure. To determine ancient longitudinal strike-slips, additional information about the deep structure is required, which can be obtained from the analysis of geophysical surveys, results of geological descriptions, and comprehensive borehole sampling. Such information is extremely limited for the studied area, and detailed maps of geophysical fields cover only small local areas of the territory. Despite this, in the used proprietary LSC software, based on an analysis of the number ratios of structures of various kinematic types, provides a conclusion regarding the presence of a strike-slip component. The conducted reconstructions of shear-related SSS for each identified scale level were checked for compliance with this condition, and in all cases, a high probability of strike-slip movements along the major structure was established. Moreover, the applied model also does not exclude the possibility of identifying more local fractures of another kinematic type relative to the strike-slip major structure (Fig. 4). Thus, in the presented study, a conclusion about the development at a specific stage of tectogenesis of extensive reverse faults of north-northwestern to submeridional strike was made. The presence of these faults is also confirmed by previously obtained results of geological mapping, as well as by local thrusts in the northwestern direction.

The created PMs (Fig. 10), despite varying degrees of detail depending on the considered scale level at which a certain stage of tectogenesis is identified, are regional and represent the first approximation to a scientifically substantiated prediction of ore localization within the area. In general terms, this models reflect the spatial convergence of the most hydraulically active segments of fault structures during an individual stage of tectogenesis, or under their combined influence. This approach made it possible to assess the significance of the identified stages and their role in ore deposition by comparing with already known ore occurrences. It is important to note that in this case, not all areas of maxima on the PMs, even at an accuracy assessment of 94% (Fig. 10G), will correspond to ore localization. However, they can be considered as favorable spatial structural-tectonophysical criteria. An ultimate conclusion on the most promising sites, in accordance with the theory of ore-forming systems, can only be made taking into account and visualizing all factors influencing ore deposition in the final model: the source, migration pathways, depositional area, and the preservation of the depositional area throughout subsequent geological history. In the considered example, it was possible to identify structural factors represented by multi-rank fault structures and their segments favorable for migration and deposition of ore mineralization. Information on sources, which within the entire considered area could be various and active during different periods of geological history, can only be obtained with the application of an extensive complex of additional methods for reconstructing physico-chemical conditions of ore genesis and deep structure. The preservation of probable ore deposition areas must also be determined through more precise reconstructions of the entire geological history, taking into account the level of erosional section from the assumed time of the ore-forming process.

The approach to creating PMs based on the data normalization procedure allows additionally integrate into the created maps any other diverse information with different spatial resolution (depending on the observation network), which is significant for predicting the localization of the target ore type. Therefore, adding spatial, more objective information would increase the prediction accuracy and enable the creation of a local model for areas where additional data are available. For example, the results of geochemical survey for at least part of the studied area would allow for the creation of a more comprehensive PM using the existing structural

models, which would be characterized by much higher predictive accuracy.

In addition, it is necessary to note that the article considers exclusively linear structures. In areas with active paleovolcanism, to which the studied territory also belongs, an important role in the localization of ore mineralization is played by so-called "structures of the central type" or "ring structures" (Soloviev, 1978). These structures can also be identified based on a structural-geomorphological approach using a DEM (Ustinov et al., 2024b). The spatial position of ring structures should be taken into account in the metallogenic analysis of the territory and in creating PMs. For this purpose, the authors have previously developed a separate methodology for interpreting their position in GIS, taking into account the formulated favorable criteria for ore deposition relative to individual structural elements of these structures. Such work is planned for further implementation.

Conclusion

The complex of remote spatial structural-geomorphological and tectonophysical studies proposed and implemented by the authors has made it possible to obtain a number of unique results for the western part of the Baikal-Patom Belt in the context of its geodynamic evolution for the purpose of predicting ore localization, and to formulate the following main conclusions.

Based on the use of DEM, procedures for its filtering in main directions, artificial reduction of its spatial resolution with a defined step, as well as developed proprietary software tools and algorithms for automatic detection, visualization, and interpretation of linear relief elements, a multi-scale approach has been formulated and applied. This approach allows for the sequential, optimal identification of groups of lineaments reflecting fault structures of various ranks, which together form the general framework of tectonic structures within the studied area. At each subsequent step of degrading the DEM spatial resolution, a decrease in the number of automatically identified linear objects and an increase in their average length were observed.

For the multi-scale groups of lineaments, rose-diagrams and relative specific density maps were constructed. Their analysis made it possible to identify the main orientation trends of the assumed fault structures and to visualize their spatial distribution depending on the rank of the identified objects.

Practically at all levels, except the most local ones, the distribution of structures is characterized by a predominantly northeastern trend. A north-northwest to sub-meridional striking system can be distinguished exclusively at supra-regional levels, while a northwestern orientation system is present at regional levels. The lowest levels demonstrate a dominance of a sub-latitudinal fault system.

The calculation of correlation coefficients between the created relative specific density maps of multi-scale lineament classes opened possibilities for their more precise grouping and attribution to a specific scale level. Consequently, local, regional, and supra-regional levels were identified.

Based on the interpretation of the orientations and lengths along the strike of the identified linear structures using the P.L. Hancock's shear model and the proprietary software "LSC", the parameters of shear-related tectonic stresses were reconstructed for each of the established scale levels. Additionally, a classification of the assumed fault structures according to kinematic type was performed. This made it possible to identify distinct, most prominent stages of the tectonic evolution of the territory.

The first stage is reconstructed for all assumed structures at all established scale levels and corresponds to the most powerful strike-slip processes. It is characterized by a sub-latitudinal to east-northeastern orientation of the maximum compression axis, the development of extensive regional and supra-regional major structures of northeastern strike as right-lateral strike-slips, reverse faults of north-northwestern and sub-meridional orientations, as well as formation of less extensive northwestern left-lateral strike-slips. This stage corresponds to the accretionary-collisional processes of attaching the BFA terranes to the Siberian craton (Late Precambrian).

The second stage is identified exclusively at the most local level and is characterized by northeastern orientation of the maximum compression axis. During this stage, structures with sublatitudinal strikes, functioning as left-lateral strike-slips, experienced the greatest development. These structures were initially formed at the previous stage as tension megacracks. Most likely, this stage is associated with processes of Early Paleozoic tectonomagmatic activation of the territory. The ore bodies of most known deposits are predominantly confined to fault structures with these orientations.

The third stage is associated with an inversion of stress-strain state parameters, when the maximum compression axis acquired a northwestern orientation. This stage is also identified only at the local level and is characterized by continuation of development of relatively short sub-latitudinal strike-slips, but with right-lateral kinematics. Under such parameters, the local thrusts in a northwestern direction towards the Siberian craton, which were mapped during earlier studies, most likely formed.

The applied approach to visualization of the most hydraulically active zones based on the calculation of the slip tendency coefficient and the construction of comprehensive prediction models for each of the identified scale levels of fault structure development at variations of stress-strain state parameters and their different combinations, made it possible to establish spatial patterns between the localization of known ore occurrences within the area and the structural-tectonic permeability during specific stages of tectogenesis, as well as their combined influence.

Based on the assessment of accuracy of each model, it has been shown that the combined action of the processes of the first and second stages of tectogenesis had the greatest influence on the deposition of ore mineralization within the studied area.

Ackmowledgements

The study was supported by the grant of the Russian Science Foundation No. 24-27-00218, https://rscf.ru/en/project/24-27-00218/.

The authors express their gratitude to the reviewers for valuable comments and suggestions that contributed to improving the work.

References

Anders M.H., Wiltschko D.V. (1994). Microfracturing, paleostress and the growth of faults. *J. Struct. Geol*, 16(6), pp. 795–815. https://doi.org/10.1016/0191-8141%2894%2990146-5

Anderson E.M. (1905). The dynamics of faulting. *Transactions of the Edinburgh Geological Society*, 8, pp. 387–402. https://doi.org/10.1144/transed.8.3.387

Andreev A.A., Rytsk E.Yu., Velikoslavinskii S.D., Tolmacheva E.V., Bogomolov E.S., Lebedeva Y.M., Fedoseenko A.M. (2022). Age, composition, and tectonic setting of the formation of late neoproterozoic (late baikalian) complexes in the Kichera zone, Baikal-Vitim belt, northern Baikal area: geological, geochronological, and Nd isotope data. *Petrology*, 30(4), pp. 337–368. https://doi.org/10.1134/s0869591122040026

Burtman V.S., Leonov Yu.G., Lukyanov A.V., Makarov V.I., Rastsvetaev L.M., Suvorov A.I., Trifonov V.G., Khain V.E., Shcherba I.G. (1980). Problems of global correlation of geological phenomena. Moscow: Nauka, 229 p. (In Russ.)

Carranza E. (2004). Weights of Evidence Modeling of Mineral Potential: A Case Study Using Small Number of Prospects, Abra, Philippines. *Natural Resources Research*, 13, pp. 173–187. http://dx.doi.org/10.1023/B:NARR.0000046919.87758.f5

Chugaev A.V., Chernyshev I.V., Dubinina E.O., Shatagin K.N., Budyak A.E., Tarasova Y.I., Skuzovatov S.Y., Gareev B.I., Goryachev N.A. (2018). Isotopic (Sm–Nd, Pb–Pb, and $\delta^{34}S$) and geochemical characteristics of the metasedimentary rocks of the Baikal–Patom belt (northern Transbaikalia) and evolution of the sedimentary basin in the Neoproterozoic. *Petrology*, 26(3), pp. 213–245. https://doi.org/10.1134/S0869591118030025

Enoh M.A., Okeke F.I., Okeke U.C. (2021). Automatic lineaments maEnoh M.A., Okeke F.I., Okeke U.C. (2021). Automatic lineaments mapping and extraction in relationship to natural hydrocarbon seepage in Ugwueme, South-Eastern Nigeria. *Geod. Cartogr.*, 47, pp. 34–44. https://doi.org/10.3846/GAC.2021.12099

Faulkner D.R., Mitchell T.M., Jensen E., Cembrano J. (2011). Scaling of fault damage zones with displacement and the implications for fault growth processes. *J. Geophys. Res. Solid Earth*, 116(5), pp. 1–11. http://dx.doi.org/10.1029/2010JB007788

Faulkner D.R., Sanchez-Roa C., Boulton C., den Hartog, S.A.M. (2018). Pore fluid pressure development in compacting fault gouge in theory, experiments, and nature. *J. Geophys. Res.: Solid Earth*, 123(1), pp. 226–241. http://dx.doi.org/10.1002/2017JB015130

Franca-Rocha W., Bonham-Carter G., Misi A. (2003). GIS modeling for mineral potential mapping of carbonate-hosted Pb-Zn deposits. *Brazilian Journal of Geology*, 33, pp. 191–196. http://dx.doi.org/10.25249/0375-7536.200333S2191196

Fuchs K., Müller B. (2001). World Stress Map of the Earth: a key to tectonic processes and technological applications. *Naturwissenschaften*, 88, pp. 357–371. https://doi.org/10.1007/s001140100253

Gitis V.G., Shchukin Yu.K., Starostin V.I. (2013). GIS technology for forecasting ore deposits. *Information Processes*, 13(2), pp. 48–63. (In Russ.) https://elibrary.ru/qynnqr

Gordienko I.V. (2006). Geodynamic evolution of the late Baikalides and Paleozoides of the folded frame of the Siberian platform. *Russian Geology and Geophysics*, 47(1), pp. 53–70. (In Russ.) https://elibrary.ru/lvhrvs

Gordienko I.V., Bulgatov A.N., Orsoev D.A. (2013). Geodynamic settings and metallogeny of the Sayan-Baikal mountain region. *Domestic Geology*, 3, pp. 7–15. (In Russ.). https://elibrary.ru/qbfnuj

Grishkov, G.A., Nafigin, I.O., Ustinov, S.A. et al. (2023). Developing a Technique for Automatic Lineament Identification Based on the Neural Network Approach. *Izv. Atmos. Ocean. Phys*. 59, pp. 1271–1280. https://doi.org/10.1134/S0001433823120101

Gusev G.S., Khain V.E. (1995). On the relationships between the Baikal-Vitim, Aldan-Stanovoy, and Mongol-Okhotsk terranes (south of Central Siberia). *Geotectonics*, 5, pp. 68–82. (In Russ.).

Gzovsky M.V. (1975). Fundamentals of tectonophysics. Moscow: Nauka, 536 p. (In Russ.).

Hancock P.L. (1985). Brittle microtectonics: principles and practice. *J. of Struct. Geol*, 7(3/4), pp. 437–457. https://doi.org/10.1016/0191-8141(85)90048-3

Hawker L., Uhe P., Paulo L., Sosa J., Savage J., Sampson C., Neal J. (2022). A 30 m global map of elevation with forests and buildings removed. *Environ. Res. Lett*., 17(2), 024016, https://doi.org/10.1088/1748-9326/ac4d4f

Hobbs W.H. (1904). Lineaments of the Atlantic Border Region. *Geological Society. American Bulletin*, 15, pp. 483–506. https://doi.org/10.1130/GSAB-15-483

Ivanov A.I., Rozhok S.N., Strakhova T.M., Yakovlev V.P. et al. (1982). Geological structure and useful minerals of the interfluve of the lower reaches of the Vitim and Bol. Patom (Report of the Tuyukan party on group geological survey at a scale of 1:50,000 for 1978-1980). Irkutsk, Inv. No. 14-78-31/24. (In Russ.)

Jaeger J.C., Cook N.G.W. (1979). Fundamentals of Rock Mechanics. 3rd edit., 593 p. http://dx.doi.org/10.1017/S001675680003274X

Kats Ya. G., Poletaev A. I., Rumyantseva E. F. (1986). Fundamentals of lineament tectonics. Moscow: Nedra, 144 p. (In Russ.)

Khomentovsky V.V., Postnikov A.A. (2001). Neoproterozoic history of the development of the Baikal-Vilyui branch of the Paleoasian Ocean. *Geotectonics*, 3, pp. 3–21. (In Russ.) http://www.ipgg.sbras.ru/ru/science/publications/publ-neoproterozoyskaya-istoriya-razvitiya-baykalo-vilyuyskoy-3321-2001

Kocharyan G.G. (2021) Nucleation and Evolution of Sliding in Continental Fault Zones under the Action of Natural and Man-Made Factors: A State-of-the-Art Review. *Izv., Phys. Solid Earth*, 57, pp. 439–473. https://doi.org/10.1134/S1069351321040066

Koveshnikov A. M., Podshivalov A. N., Pimnev Yu. K. et al. (1989). Prospective zoning of the Tonodskoye Uplift territory for uranium with the selection of areas and objects for detailed prospecting and evaluation work based on structural-geological, radiogeochemical, mineralogical-petrographic studies, interpretation of space and aerial photographs and revision of known uranium manifestations with the compilation of a prospective zoning scheme on a scale of 1:200,000 over an area of 7.5 thousand square kilometers. According to geological assignment 5-1 for 1985-1989. Irkutsk, RGF No. 2698. (In Russ.).

Kuzmin M.I., Yarmolyuk V.V. (2016). Plate tectonics and mantle plumes - the basis of endogenous tectonic activity of the Earth over the past 2 billion years. *Russian Geology and Geophysics*, 57(1), pp. 8–21. https://doi.org/10.1016/j.rgg.2016.01.002

Kuzmin Yu.O. (2018). Modern anomalous deformations of the earth's surface in fault zones: shear or extension? *Geodynamics and Tectonophysics*, 9(3), pp. 967–987. (In Russ.). https://doi.org/10.5800/GT-2018-9-3-0379

Makarev L.B., Mironov Yu.B. (2014). Features of metallogeny and prospects for industrial uranium-bearing capacity of the Chuya-Tonod mineragenic zone of northern Transbaikalia (based on GK-1000/3 and GDP-200/2 materials). *Regional Geology and Metallogeny*, 57, pp. 87–94. (In Russ.).

Makarev L.B., Mitrofanov G.L., Mitrofanova N.N., Pai V.M., Semeykina L.K. et al. (2010). State Geological Map of the Russian Federation at a scale of 1:1,000,000 (third generation). Aldan-Transbaikal Series. Sheet O-50 -

Bodaibo. Explanatory note. St. Petersburg: VSEGEI Cartographic Factory, 612 p. (In Russ.)

Makarov V.I. (2008). Quaternary tectonics and geodynamics of platform territories: current problems of study. *Byulleten" Komissii Po Izucheniyu Chetvertichnogo Perioda*, 68, pp. 10–25. (In Russ.). https://www.elibrary.ru/wfloed

Minaev V.A., Ustinov S.A., Petrov V.A., Svecherevsky A.D., Nafigin I.O. (2024a). Regional remote sensing analysis of fault tectonics of the Kola Peninsula and its role in ore formation. *Russian Journal of Earth Sciences*, 24(3), ES3010. (In Russ.). https://doi.org/10.2205/2024ES000918

Minaev V.A., Ustinov S.A., Petrov V.A. Svecherevsky A.D., Nafigin I.O. (2024b). Regional Remote Sensing Analysis of Fault Tectonics of the Taimyr–Severozemel Orogen and Its Role in Ore Formation. *Izv. Atmos. Ocean. Phys.*, 60, pp. 1566–1578. https://doi.org/10.1134/S0001433825700227

Mitrofanova N.N., Boldyrev V.I., Korobeynikov N.K., Mitrofanov G.L. et al. (2012). State Geological Map of the Russian Federation. Scale 1:1,000,000 (third generation). Aldan-Transbaikal Series. Sheet O-49 – Kirensk. Explanatory Note. St. Petersburg: VSEGEI Cartography Factory, 607 p. (In Russ.)

Nikishin A.M., Sobornov K.O., Prokopyev A.V., Frolov S.V. (2010). Tectonic evolution of the Siberian Platform during the Vendian and Phanerozoic. *Moscow Univ. Geol. Bull*., 65, pp. 1–16. https://doi.org/10.3103/S0145875210010011

Paplinski A. (1998). Directional filtering in edge detection. *IEEE Trans. Image Processing*, 7, pp. 611–615. http://dx.doi.org/10.1109/83.663510

Petrov V.A., Lespinasse M., Poluektov V.V., Ustinov S.A., Minaev V.A. (2017). Rescaling of fluid-conducting fault structures. *Doklady Earth Sciences*, 472(2), pp. 130–133. https://doi.org/10.1134/S1028334X17020027

Petrov V.A., Lespinasse M., Poluektov V.V., Ustinov S.A., Minaev V.A. (2019). Scale effect in a fluid-conducting fault network. *Geology of ore deposits*, 61(4), pp. 293–305. https://doi.org/10.1134/S1075701519040056

Petrov V.A., Sim L.A., Nasimov R.M., Shchukin S.I. (2010). Fault tectonics, neotectonic stresses, and hidden uranium mineralization in the area adjacent to the Strel'tsovka caldera. *Geology of Ore Deposits*, 52(4), pp. 279–288. https://doi.org/10.1134/S1075701510040033

Porwal A., González-Álvarez I., Markwitz V., McCuaig T.C., Mamuse A. (2010). Weights-of-evidence and logistic regression modeling of magmatic nickel sulfide prospectivity in the Yilgarn Craton, Western Australia. *Ore Geology Reviews*, 38(3). pp. 184–196. http://dx.doi.org/10.1016/j.oregeorev.2010.04.002

Rats M.V., Chernyshev S.N. (1970). Fracturing and properties of fractured rocks. Moscow: Nedra, 160 p. (In Russ.).

Rebetsky Yu. L., Kuchai O. A., Sycheva N. A. (2009). Method of cataclastic analysis of faults and results of calculations of the modern stress state in the crust near plate boundaries and for intraplate mountain-folded orogens. *Tectonophysics and topical issues of earth sciences for the 40th anniversary of the creation of the tectonophysics laboratory at the IPE RAS by M. V. Gzovsky: materials of reports of the All-Russian conference*. Moscow: IPE RAS, Vol. 1, pp. 340–366. (In Russ.). http://www.gdirc.ru/files/structure/Scientific_Projects/rffi-09-05-00687-a/articles/Rebetsky.pdf

Rebetsky Yu.L. (2008). Mechanism of generation of tectonic stresses in areas of large vertical movements. *Physical Mesomechanics*, 1(11), pp. 66–73. (In Russ.). https://doi.org/10.1016/j.physme.2008.03.008

Rebetsky Yu.L., Sim L.A., Marinin A.V. (2017). From slickensides to tectonic stresses. Methods and algorithms. Moscow: GEOS, 235 p. (In Russ.). https://elibrary.ru/YPNZQR

Riedel W. (1929). Zur Mechanik Geologischer Brucherschei-nungen. *Zbl. Mineralogie, Geol. Und Palaentol., Abt. B*., pp. 354–368.

Rytsk E.Y., Kovach V.P., Bogomolov E.S., Kotov A.B., Yarmolyuk V.V., Kovalenko V.I. (2011). Isotopic structure and evolution of the continental crust in the east Transbaikalian segment of the Central Asian foldbelt. *Geotectonics*, 45(5), pp. 349–377. https://doi.org/10.1134/S0016852111050037

Rytsk E.Yu. (2020). Tectonic zoning of the Baikal folded region and stages of its formation. Fundamental problems of tectonics and geodynamics. *Proceedings of the LII Tectonic Conference*. Moscow: GEOS, Vol. 2, pp. 256–259. (In Russ.). https://elibrary.ru/eelpcd

Salop L.I. (1964). Geology of the Baikal mountain region. Moscow: Nedra, Vol. 1, 515 p. (In Russ.)

Shahi H., Rouhani A.K.A. (2014). GIS-based weights-of-evidence model for mineral potential mapping of hydrothermal gold deposits in Torbat-e-Heydarieh area. *Journal of Mining and Environment*, 5, pp. 79–89. https://doi.org/10.22044/jme.2014.324

Sherman S.I. (2014). Seismic process and earthquake prediction: tectonophysical concept. Novosibirsk: Geo, 359 p. (In Russ.)

Sherman S.I., Bornyakov S.A., Buddo V.Yu. (1983). Areas of dynamic influence of faults (modeling results). Novosibirsk: Nauka, 110 p. (In Russ.)

Shmankevich A.Yu., Melnikov I.D. et al. (1983). Report on the results of geological and geophysical exploration work in the western part of the Tonod anticlinorium (Northern party of the Meget expedition, 1980-83). RGF No. 404197. (In Russ.)

Smirnov V.I. (1976). Geology of useful minerals. Moscow: Nedra, 688 p. (In Russ.)

Soloviev V.V. (1978). Structures of the central type of the territory of the USSR according to geological and morphological analysis. Explanatory note to the Map of morphostructures of the central type of the territory of the USSR on a scale of 1: 10,000,000. Leningrad: Ministry of Geology of the USSR. All-Union Order of Lenin scientific research geol. int., 111 p. (In Russ.)

Stanevich A.M., Mazukabzov A.M., Postnikov A.A. et al. (2007). Northern segment of the Paleoasian Ocean: Neoproterozoic deposition history and geodynamics. *Russian Geology and Geophysics*, 48(1), pp. 46–60. https://doi.org/10.1016/j.rgg.2006.12.005

Suzen M.L., Toprak V. (1998). Filtering of Satellite Images in Geological Lineament Analyses: An Application to a Fault Zone in Central Turkey. *Int. J. Remote Sens*, 19. pp. 1101–1114. https://doi.org/10.1080/014311698215621

Ustinov S.A., Chepchugov A.M., Tomarovskaya M.A.,Petrov V.A., Svecherevskiy A. D., Yarovaya E.V. (2024a). Structural–Tectonophysical Approach to Interpreting Lineament Analysis Results for the Prediction of Ore-Forming Mineral Systems Using the Example of the Tuyukan Ore Cluster Area. *Izv. Atmos. Ocean. Phys.*, 60, pp. 1547–1565. https://doi.org/10.1134/S0001433825700215

Ustinov S.A., Petrov V.A. (2016). Using detailed digital elevation models for structural-lineament analysis (using the Urtuy granite massif, southeastern Transbaikalia as an example). *Geoinformatics*, 2, pp. 51–60. (In Russ.) https://geoinformatika.ru/?page_id=4051

Ustinov S.A., Petrov V.A., Minaev V.A., Nafigin I.O., Yarovaya E.V. (2024b). Detection and interpretation of central type structures within the territory of southeastern Transbaikalia for prediction of ore-forming systems. *Geology of ore deposits*, 66(4), pp. 345–375. http://dx.doi.org/10.1134/S107570152460018X

Vidyapin Yu.P., Bondar I.V. (2021) Possibilities of using lineament analysis of the Earth's surface relief for geodynamic studies using the Caucasus region as an example. *Bulletin of the Moscow Society of Naturalists. Geological Department*, 96(2), pp. 39–51. (In Russ.)

Wilson J.E., Chester J.S., Chester F.M. (2003). Microfracture analysis of fault growth and wear processes, Punchbowl Fault, San Andreas System, California. *J. Struct. Geol*, 25, pp. 1855–1873. http://dx.doi.org/10.1016/S0191-8141(03)00036-1

Zobak M.D. (2018). Geomechanics of oil deposits. Izhevsk: Institute of Computer Research, 479 p. (In Russ.).

Zonenshain L.P., Kuzmin M.I., Natapov L.M. (1990). Tectonics of lithospheric plates on the territory of the USSR. Moscow: Nedra, Book. 1, 327 pp. (In Russ.)

Zorin Yu.A., Sklyarov E.V., Belichenko V.G., Mazukabzov A.M. (2009). Island arc–back-arc basin evolution: implications for Late Riphean–Early Paleozoic geodynamic history of the Sayan–Baikal folded area. *Russian Geology and Geophysics*, 50(3), pp. 149–161. https://doi.org/10.1016/j.rgg.2008.06.022

About the Authors

Stepan A. Ustinov – Cand. Sci. (Geology and Mineralogy), Deputy Director for Science, Institute of Geology of Ore Deposits, Petrography, Mineralogy and Geochemistry of the Russian Academy of Sciences

35/7 Staromonetny lane, Moscow, 119017, Russian Federation

e-mail: stevesa@mail.ru

Vladislav A. Petrov – Doctor Sci. (Geology and Mineralogy), Corresponding Member of the Russian Academy of Sciences, Director, Institute of Geology of Ore Deposits, Petrography, Mineralogy and Geochemistry of the Russian Academy of Sciences

35/7 Staromonetny lane, Moscow, 119017, Russian Federation

e-mail: vlad243@igem.ru

Anton A. Andreev – Cand. Sci. (Geology and Mineralogy), Researcher of the Laboratory of Rare-Metal Magmatism, Institute of Geology of Ore Deposits, Petrography, Mineralogy and Geochemistry of the Russian Academy of Sciences

35/7 Staromonetny lane, Moscow, 119017, Russian Federation

e-mail: axel-foley@yandex.ru

Aleksey Dz. Svecherevsky – Junior Researcher of the Laboratory of Geoinformatics, Institute of Geology of Ore Deposits, Petrography, Mineralogy and Geochemistry of the Russian Academy of Sciences

35/7 Staromonetny lane, Moscow, 119017, Russian Federation

e-mail: alexey@svecherevskiy.ru

Igor A. Kochkin – Postgraduate Student, Junior Researcher of the Laboratory of Geoinformatics, Institute of Geology of Ore Deposits, Petrography, Mineralogy and Geochemistry of the Russian Academy of Sciences

35/7 Staromonetny lane, Moscow, 119017, Russian Federation

e-mail: iakochkin@yandex.ru

Vladimir V. Shukhov – Assistant-Researcher of the Laboratory of Geoinformatics, Institute of Geology of Ore Deposits, Petrography, Mineralogy and Geochemistry of the Russian Academy of Sciences

35/7 Staromonetny lane, Moscow, 119017, Russian Federation

e-mail: vladimirsh3993@gmail.com

Manuscript received 17 March 2025;
Accepted 23 July 2025;
Published 20 December 2025

IN RUSSIAN

Интерпретация линеаментов в пределах западной части Байкало-Патомского пояса с применением мультимасштабного тектонофизического подхода в контексте прогноза рудообразующих систем

С.А. Устинов, В.А. Петров, А.А. Андреев, А.Д. Свечеревский, И.А. Кочкин, В.В. Шухов*
Институт геологии рудных месторождений, петрографии, минералогии и геохимии РАН, Москва, Россия
** Ответственный автор: Степан Андреевич Устинов, e-mail: stevesa@mail.ru*

В статье на примере территории западной части Байкало-Патомского пояса на основе последовательного занижения пространственного разрешения цифровой модели рельефа FABDEM предложен авторский подход к автоматическому выделению линеаментов, отражающих различные масштабные уровни развития каркаса разрывных нарушений. Представлены результаты комплексного пространственно-геометрического анализа выделенных линеаментов, маркирующих разноранговые разрывные структуры. На основе корреляционного анализа выделены группы структур, однозначно отвечающих определённому масштабному уровню. Для реконструкции параметров напряженно-деформированного состояния, кинематики предполагаемых разрывных структур и восстановления последовательности этапов тектогенеза, парагенезис выделенных на каждом этапе генерализации цифровой модели рельефа структур интерпретировался на основе модели сдвига, предложенной П.Л. Хэнкоком. В результате в истории геологического развития территории установлены три последовательных этапа тектогенеза, характеризующихся: I) субширотной – восток-северо-восточной, II) северо-восточной и III) северо-западной ориентировками оси максимального сжатия. Первый этап проявлен на всех масштабных уровнях и отвечает процессам аккреционно-коллизионного взаимодействия окраины Сибирского кратона с микроконтинентами и островодужными террейнами. Второй и третий этапы проявлены исключительно на локальном уровне и коррелируют с формированием субширотных сдвигов и надвигов в северо-западном направлении. Полученные результаты на основе расчета коэффициента тенденции к сдвигу и визуализации наиболее гидравлически активных сегментов разрывных структур легли в основу создания разномасштабных прогнозно-поисковых моделей полезных ископаемых территории с учетом выявленных этапов тектогенеза. Установлено, что наибольшую роль в локализации металлического оруденения сыграли первый и второй этапы. В этом случае точность комплексной модели составила 94%.

Ключевые слова: дистанционное зондирование Земли, цифровая модель рельефа, линеаментный анализ, разлом, тектонофизический анализ, структурно-геоморфологический метод, напряженно-деформированное состояние, прогнозно-поисковая модель полезных ископаемых, Байкальская складчатая область, Байкало-Патомский пояс

Для цитирования: Устинов С.А., Петров В.А., Андреев А.А., Свечеревский А.Д., Кочкин И.А., Шухов В.В. (2025). Интерпретация линеаментов в пределах западной части Байкало-Патомского пояса с применением мультимасштабного тектонофизического подхода в контексте прогноза рудообразующих систем. *Георесурсы,* 27(4), с. 83–106. https://doi.org/10.18599/grs.2025.4.7